EBioMedicine 32 (2018) 142–163

Contents lists available at ScienceDirect

EBioMedicine

journal homepage: www.ebiomedicine.com

Research Paper

Comprehending a Killer: The Akt/mTOR Signaling Pathways Are Temporally High-Jacked by the Highly Pathogenic 1918 Influenza Virus

Charlene Ranadheera [a,b], Kevin M. Coombs [a,c,d,*], Darwyn Kobasa [a,b,**]

[a] Department of Medical Microbiology, Faculty of Medicine, University of Manitoba, Winnipeg, Manitoba R3E 0J6, Canada
[b] Special Pathogens Program, National Microbiology Laboratory, Public Health Agency of Canada, Winnipeg, Manitoba R3E 3R2, Canada
[c] Manitoba Centre for Proteomics & Systems Biology, Room 799, 715 McDermot Avenue, Winnipeg, Manitoba R3E 3P4, Canada
[d] Manitoba Institute of Child Health, John Buhler Research Centre, Room 513, 715 McDermot Avenue, Winnipeg, Manitoba R3E 3P4, Canada

ARTICLE INFO

Article history:
Received 15 February 2018
Received in revised form 8 May 2018
Accepted 21 May 2018
Available online 2 June 2018

Keywords:
RNA virus
Virus infection
Host cell alterations
Mass spectrometry
Liquid chromatography
Bioinformatics

ABSTRACT

Previous transcriptomic analyses suggested that the 1918 influenza A virus (IAV1918), one of the most devastating pandemic viruses of the 20th century, induces a dysfunctional cytokine storm and affects other innate immune response patterns. Because all viruses are obligate parasites that require host cells for replication, we globally assessed how IAV1918 induces host protein dysregulation. We performed quantitative mass spectrometry of IAV1918-infected cells to measure host protein dysregulation. Selected proteins were validated by immunoblotting and phosphorylation levels of members of the PI3K/AKT/mTOR pathway were assessed. Compared to mock-infected controls, >170 proteins in the IAV1918-infected cells were dysregulated. Proteins mapped to amino sugar metabolism, purine metabolism, steroid biosynthesis, transmembrane receptors, phosphatases and transcription regulation. Immunoblotting demonstrated that IAV1918 induced a slight up-regulation of the lamin B receptor whereas all other tested virus strains induced a significant down-regulation. IAV1918 also strongly induced Rab5b expression whereas all other tested viruses induced minor up-regulation or down-regulation. IAV1918 showed early reduced phosphorylation of PI3K/AKT/mTOR pathway members and was especially sensitive to rapamycin. These results suggest the 1918 strain requires mTORC1 activity in early replication events, and may explain the unique pathogenicity of this virus.

1. Introduction

The 1918 influenza pandemic was one of the most devastating infectious disease events of the 20th century, resulting in 20–100 million deaths [56,86]. Although the young and the elderly are usually the most susceptible to influenza A virus (IAV) epidemics and many pandemics, the 1918 pandemic was unusual in that a much larger proportion of healthy young adults succumbed to the infection [86], which has been attributed to a dysfunctional host immune response (cytokine storm) [47,53]. A link between the cytokine storm and IAV-induced pathogenesis and poor clinical outcome has long been appreciated [1,47,49,61,87]. Recent attempts to modulate the cytokine storm, including using lipid-modifying compounds such as sphingosine-1-phosphate [60,61,91] have been only partially successful. Because all viruses are obligate parasites that require a host cell in which to replicate, a more complete and detailed understanding of cell signaling and how IAV induces host protein dysregulation is required (recently reviewed in [87]).

The need to better delineate host responses to IAV infection is further underscored by the nature of the virus. IAV is a small, enveloped virus in the family *Orthomyxoviridae*, with a genome of 8 negative-sense single stranded RNA segments that encode for at least 15 proteins [39,62]. IAV have enormous genetic plasticity, mediated by nucleotide (genetic drift) and genome segment exchange (genetic shift), changes that control differences in host range and virulence. IAV are serologically categorized by the hemagglutinin (HA) and neuraminidase (NA) proteins, both of which are located in the viral envelope. There are currently 18 recognized HA (H1–H18) and 11 NA (N1–N11) types [62,65,89]. Various anti-viral strategies, including small molecule inhibitors and vaccines, have been developed to combat IAV. However, the virus' genetic plasticity often leads to resistance rapidly developing to these virus-targeted anti-viral modalities. In addition, because of the virus' enormous host range, spanning avian, marine mammals and numerous land animals including humans, eradication of the virus is extremely unlikely.

Environmental stressors, including virus infection, induce a number of alterations in a host cell's transcriptome and proteome. Previous

* Correspondence to: K. M. Coombs, Manitoba Centre for Proteomics & Systems Biology, University of Manitoba, Winnipeg, MB, Canada.
** Correspondence to: D. Kobasa, National Microbiology Laboratory, Public Health Agency of Canada, Winnipeg, MB, Canada.
E-mail addresses: kevin.coombs@umanitoba.ca, (K.M. Coombs), darwyn.kobasa@phac-aspc.gc.ca (D. Kobasa).

https://doi.org/10.1016/j.ebiom.2018.05.027

transcriptomic analyses of cellular responses to IAV have provided some information (for example: [2,28]), including description of innate immune response patterns in macaques infected with the 1918 influenza strain [47]. However, there often is poor concordance between microarray and protein data [2,57,88], partly because mRNA levels cannot provide complete information about extents of post-translational modifications or about levels of effector protein synthesis.Thus, we complemented some of our previous transcriptomic analyses of 1918 virus infection [47] by using a non-biased stable isotope-based quantitative mass spectrometric method to globally assess host proteomic alterations induced by 1918 virus infection in cultured A549 cells.

2. Materials and Methods

2.1. Cells and Viruses

2.1.1. Viruses

All viruses used in this study (Supplementary Table S1), including IAV strain A/South Carolina/1/1918 (H1N1; "1918"), were generated by reverse genetics as previously described [59]. All infectious work was carried out under containment level 4 (CL-4) conditions at the National Microbiology Laboratory in Winnipeg, Canada as outlined in the Health Canada Laboratory Bio-safety Guidelines CL-4 handling procedures (www.hc-sc.gc.ca/pphb-dgspsp/publicat/lbg-ldmbl-96/index.html).

2.1.2. Cells

Human lung A549 cells (American Type Culture Collection # CCL-185) and Madin Darby canine kidney (MDCK) (ATCC # CCL-34) cells were routinely cultured in Dulbecco's modified MEM (DMEM) supplemented with non-essential amino acids, sodium pyruvate, 0.2% (*w*/*v*) glucose, 10% fetal bovine serum (FBS; Invitrogen), and 2 mM L-glutamine as previously described[12]. To label A549 cells with SILAC for global non-biased quantitative proteomic analyses, they were grown in DMEM media provided with a SILAC™ Phosphoprotein Identification and Quantification Kit (Invitrogen Canada Inc.; Burlington, Ontario), supplemented as above (except without non-essential amino acids), and with 10% dialyzed FBS (Invitrogen Canada Inc.; Burlington, Ontario), plus 100 mg each of "light" (**L**; $^{12}C_6/^{14}N_4$) or "heavy" (**H**; $^{13}C_6/^{15}N_4$) L-lysine and l-arginine per liter of D-MEM, such that **H** isotopic forms have 6.0 and 10.0 Da heavier masses than the corresponding **L** forms [12].Virus stocks were generated, and virus titrations were performed, in MDCK cells as previously described [12].

2.1.3. Infection

Once A549 cells destined for SILAC labeling had grown through six doublings, **L** cells in 2 experiments were infected with 1918 at a multiplicity of infection (MOI) of 7 plaque forming units (PFU) per cell and an equivalent number of **H** cells were mock infected as control. Labels were swapped in the 3rd biologic replicate. Cells were overlaid with appropriate media and cultured for 5 (early) and 24 (late) hours.

All other A549 infections were performed in DMEM supplemented with 0.1% BSA and 0.5 μg/ml TPCK-Trypsin.

2.2. Cell Viability Assays

A549 cells were infected with 1918 at a MOI of 7 PFU/cell. At 5, 24 and 48 h post-infection, the media was removed and replaced with fresh OptiMEM (Life Technologies, Burlington, ON, Canada) supplemented with XTT (XTT-based InVitro Toxicology Assay Kit, Sigma-Aldrich, Oakville, Ontario, Canada) as per the manufacturer's directions. The cells were incubated for an additional 3 h. The colorimetric change was read at an absorbance of 450 nm and percent viability was normalized to the control samples. Experiments were performed in triplicate. In parallel, cells were visualized by light microscopy for the presence of cytopathic effect.

2.3. Cell Fractionation

At 5 and 24 h post-infection (hpi), **L** and **H** cells were collected and counted. Equivalent numbers of **L** and **H** cells were mixed together, mixed cells were washed 3× in >50 volumes of ice-cold Phosphate Buffered Saline (PBS), washed cells were lysed with 0.5% NP-40 supplemented with 1.1 μM pepstatin A, incubated on ice for 30 min, and nuclei removed by pelleting at 5000 ×*g* for 10 min. Nuclei were processed by a previously-described high salt/urea double extraction procedure [48] and both fractions frozen at −80C until further processing. Fractionated samples were probed with antibodies targeting nuclear and cytoplasmic proteins to ensure the method for fractionation was complete (Fig. 5A).Histone H3 is a nuclear protein, Lamin is predominantly found in the nuclear envelope, Actin is typically found in the cytoplasm and tubulin is found in both the nucleus and cytoplasm.

2.4. Mass Spectrometric Sample Preparation and Analysis

Protein content in the various fractions was determined using a BCA™ Protein Assay Kit (Pierce; Rockford, IL) and BSA standards. Samples were then reduced, alkylated and digested with trypsin as previously described[12]. Digested peptides were separated by 2D RP (reversed-phase) high pH – RP low pH peptide fractionation [29,83], and analyzed on a QStar Elite mass spectrometer (Applied Biosystems, Foster City, CA) run in a data-dependent MS/MS acquisition mode as previously described using the manufacturer's "smart exit" (spectral quality 5) settings [12]. Previously targeted parent ions were excluded from repetitive MS/MS acquisition for 60 s (50 mDa mass tolerance). Protein Pilot 2.0 (Applied Biosystems) software was used for protein identification and quantitation.Raw data files (30 in total for each run) were submitted for simultaneous search using standard SILAC settings for QStar instruments. Proteins for which at least 2 fully trypsin digested **L** and **H** peptides were detected at >99% confidence were used for subsequent comparative quantitative analysis. Raw MS data files were analyzed by Protein Pilot®, version 2.0, using the non-redundant human gene database. Proteins, and their confidences and **L:H** ratios, were returned with Geninfo Identifier (gi) numbers. Differential regulation within each experimental dataset was determined by *Z*-score normalization of each dataset, using a confidence of >1.960σ as previously described [12].

2.5. Cellular Protein Expression

A549 cells were seeded 24 h prior to use so that they were 80% confluent at the time of infection. Cells were washed with DMEM supplemented with 0.1%BSA and infected at an MOI of 7 for 1 h. The virus inoculum was removed, cells were washed with PBS, and fresh DMEM supplemented with 0.1% BSA and 0.5 μg/ml TPCK-trypsin was added to the cells. Cells were harvested at 5 h and 24 h post infection. Total cell lysates were collected by washing the cells once with PBS and lysing cells with 2% SDS for immunoblot analysis. Fractionated lysates were harvested by washing the cells with PBS, adding 0.5% NP40 supplemented with Complete Protease Inhibitor (Roche) to the cells and incubating on ice for 30 min. The lysates were then collected and centrifuged at 2500 ×*g* for 10 min to generate soluble cytoplasmic and pelleted nuclear fractions. Each fraction was brought up to equal volumes with a final concentration of 2% SDS for gel electrophoresis and immunoblot analysis. Immunoblots were performed using commercially available primary antibodies coupled with secondary antibodies containing a conjugated IRdye® (Supplementary Table S2). Blots were visualized using a Licor® Odyssey scanner. Band intensities were quantified by densitometry using ImageJ software and normalized to the expression levels of actin. Each experiment was replicated at least 3 times, the means and standard errors are graphically presented. A one-way Anova with a Dunnett post-test was used to determine any significant changes between the various virus strains tested, and a one-way

Anova with a Bonferroni post-test was used to determine any significant changes between the fractions tested.

2.6. mTOR/AKT Pathway Analysis

A549 cells were seeded 24 h prior to use so that they were 80% confluent at the time of infection.Cells were washed with DMEM supplemented with 0.1%BSA and infected at an MOI of 7 for one hour. The virus inoculum was removed, cells were washed with PBS, and fresh DMEM supplemented with 0.1% BSA and 0.5 μg/ml TPCK-trypsin was added to the cells. Cells were harvested at 5 and 24 hpi. Media were removed and the cells were washed with PBS. Ice-cold 1× MILLIPLEX® MAP Lysis Buffer(EMD Millipore, Merck KGaA, Darmstadt, Germany) was added to the cells. Cells were collected and incubated at 4 °C with gentle rocking for 10–15 min. Viruses in samples were inactivated by 5MRADS of gamma irradiation for safe removal from BSL-4. Samples were clarified by centrifugation at 2500 ×*g* for 10 min and protein content was determined using the Qubit Protein Assay Quantification Kit (Life Technologies) as per manufacturer's recommendations. The phosphorylation states of various proteins from the mTOR/AKT signaling pathway and of NFκB were determined using the Milliplex MAP Akt/mTOR Phosphoprotein 11-plex Magnetic Bead Kit and the Milliplex MAP Phospho-NFκB (Ser536) Magnetic Bead MAPmate (Life Technologies) as per manufacturer's instructions. The bead counts were normalized to protein concentrations and the means and standard errors were calculated. Each of three biologic assays was run in triplicate. Results were compared to mock-infected samples at their respective time points and a *t*-test was used to determine their significance.

2.7. Rapamycin Treatment and Viral Replication Analysis

A549 cells were seeded 24 h prior to use so that they were 80% confluent at the time of infection.Cells were washed with DMEM supplemented with 0.1%BSA and infected at an MOI of 0.01 for 1 h. The virus inoculum was removed, cells were washed with PBS, and fresh DMEM supplemented with 0.1% BSA, 0.5 μg/ml TPCK-trypsin and (0–10 nM) rapamycin was added to the cells. Media were replaced at 5 or 24 hpi with fresh DMEM supplemented with 0.1% BSA and 0.5μg/ml TPCK-trypsin. Infections were allowed to continue for a total of 48 h.Supernatants were harvested and viral titers were quantified by an endpoint Spearman-Karber $TCID_{50}$ calculation. Using GraphPad's model comparison analysis, the results were compared to two models, a horizontal line, which indicates that there are no changes in response to rapamycin treatment, and a 4-parameter dose-response curve, where rapamycin has a dose-dependent effect on viral replication. The predicted model and its probability of being correct was reported.

3. Results

3.1. Influenza Virus Infection Induces Significant Up- and Down-Regulation of Numerous Cellular Proteins

A549 cells were infected with the highly pathogenic 1918 influenza virus strain (IAV1918).Preliminary analyses of cell viability throughout infection indicated that 24 hpi was the optimal time to process the cells for analysis, since signs of infection were present but the majority of cells were still viable (Fig. 1A and B). Furthermore, immunostaining for viral non-structural protein 1 (NS1) confirmed that >80% of cells were infected by this time under our experimental conditions (Fig. 1C). Thus, we selected 5 hpi as an early time point and 24 hpi as a later time point for analyses.

Infected and mock-infected cells were harvested, separated into nuclear and cytoplasmic fractions, and lysates were processed for mass spectrometry analyses. Each experimental analysis identified ~ 1350–2050 proteins in the cytoplasmic fractions and ~ 450–950 proteins in the nuclear fractions at ≥99% confidence and with ≥2 peptides (Fig. 2A), leading to the overall identification of 3020 proteins from 113,485 **L:H** peptide pairs. The significance of protein dysregulation was assessed by multiple means. Significance of proteins detected multiple times were determined by *t*-test. In addition, to facilitate inter-experiment comparisons, and to assess significance of proteins detected only a single time, but with ≥2 non-redundant peptides, all **L:H** ratios were converted into *Z*-scores to determine each protein's quantitative deviation from each population's mean as described [12]. Protein dysregulation was considered significant if t-test *p* values were <0.05. Protein dysregulation was also considered significant if the protein was detected and measured multiple times and each of its Z-scores were ≥1.960σ or ≤−1.960σ (=95% confidence). Z-scores ≥ 2.576σ or ≤−2.576σ (=99% confidence) were considered significant if proteins were detected and measured only a single time. For further stringency, average fold-change cut-offs of ±50%, which resulted in fold-change ≥ 1.5-fold, if upwards, or ≤0.667-fold, if downward, compared to mock were applied to proteins detected multiple times and fold-change cut-offs of ±75%, representing ≥1.75-fold if upwards or ≤0.5714-fold if downward compared to mock were applied to proteins detected only a single time. Label swapping identified 24 proteins (including keratins, S100 calcium binding proteins, and albumin pre-protein) that were significantly regulated in one direction under one **L:H** labeling condition, but significantly regulated in the opposite direction under reciprocal labeling conditions and which thus likely represent contaminants; these were computationally removed from the dataset and from further consideration as described [48].

By using these *Z*-score criteria and removal of probable contaminants, we identified a total of 79 proteins that were significantly up-regulated at either 5 or 24 hpi in either the cytoplasmic or nuclear fractions and 98 proteins that were significantly down-regulated (Table 1). A few proteins were found significantly regulated in multiple time points or sub-cellular fractions. For example, the 205kD nucleoporin (Nup205) protein was up-regulated in the cytoplasmic fraction at both 5 and 24 hpi, SC11A was up-regulated at 24 hpi in both the cytoplasmic and nuclear fractions, the lamin B receptor (LBR) was up-regulated in nuclear fractions at both 5 and 24 hpi, and the β-induced transforming growth factor (BGH3) was down-regulated at 5 hpi in both the cytoplasm and nucleus (Table 1). A few proteins (H2B1C, SPD2B, RFC5, RM04, IBP7, and RAB3B) were consistently up-regulated in one sample but consistently down-regulated at either another time point or in another sub-cellular fraction, suggesting either temporal or spatial re-distribution.

Up-regulated proteins are associated with responses to stress, stimulus and virus, acetylation, cell structure, defense responses, and protein binding, whereas down-regulated proteins are associated with alternative splicing, localization, transport, protein binding, and nucleoside, nucleotide and nucleic acid metabolism.

Proteins, and their levels of regulation, were analyzed by DAVID [17,36,37] and by Ingenuity Pathways Analysis (IPA). These analyses measured numerous classes of proteins (Fig. 3A, left). While many members of most classes of proteins were up or down-regulated at 5 hpi, it is striking that all proteins in the phosphatases, kinases, transmembrane receptors, and translation regulator classes were upregulated, while all cytokines and a predominant fraction of transporters were downregulated (Fig. 3A, middle). By 24 hpi, there was a very evident shift in the expression patterns for members of some classes of proteins. For instance, transcription regulators, which showed mixed up or down regulation at the early time point were exclusively down-regulated at 24 hpi. Transmembrane receptors and translation regulators that were all up-regulated at 5 hpi were all down-regulated by 24 hpi, while most kinases, which were all up-regulated at 5 hpi were mostly down-regulated by 24 hpi. The phosphatases were further enriched among the up-regulated proteins by 24 hpi. IPA identified 10 pathways with 5 or more focus molecule members identified from SILAC analysis among the regulated proteins. The top 5 pathways, each with 14 or more identified molecules, were cellular movement,

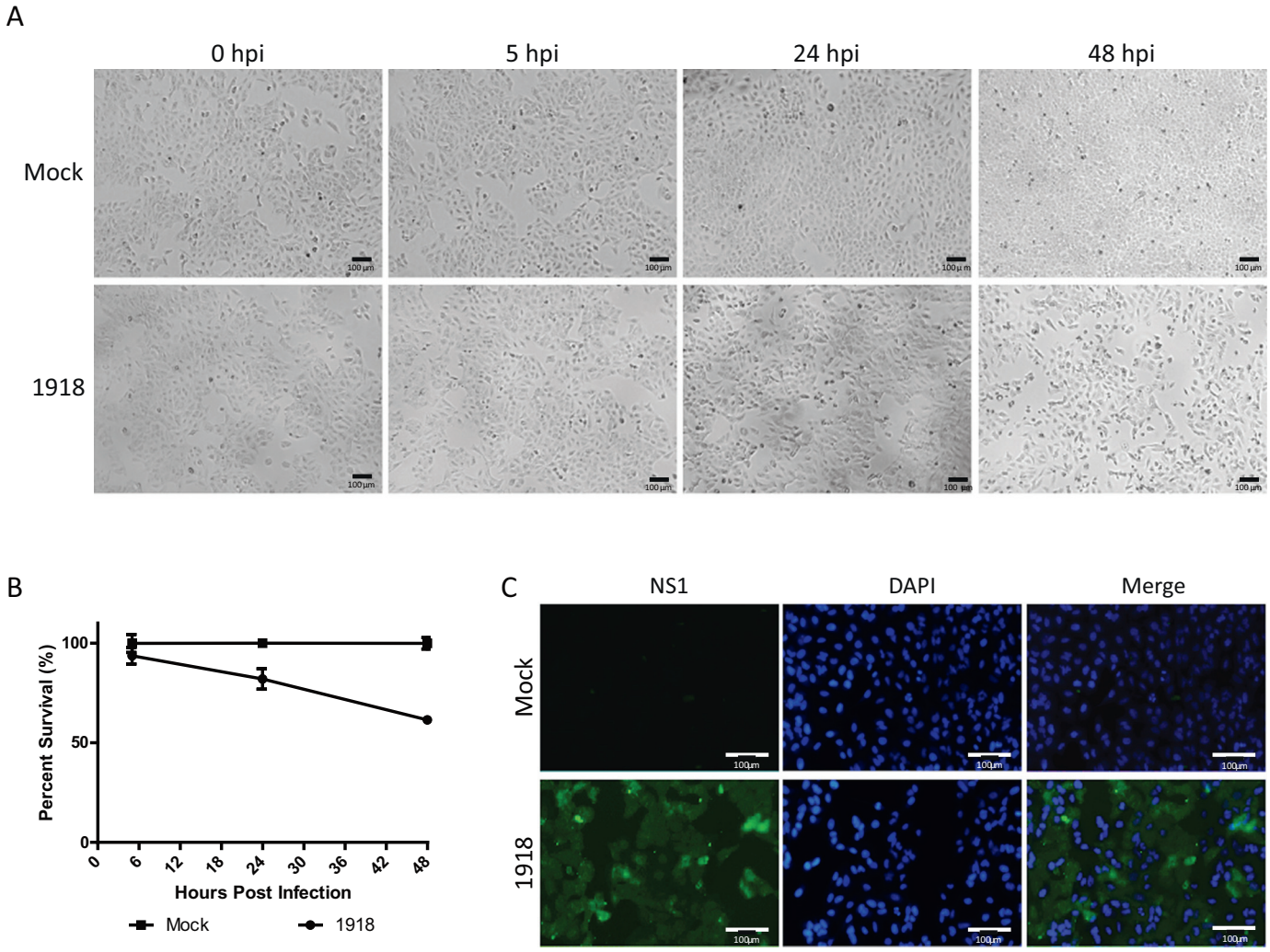

Fig. 1. Cell viability and 1918 infectivity. A549 cells were infected with 1918 at an MOI of 7 and harvested at 5, 24, and 48 h post-infection. (A) Cells were visualized by bright-field microscopy and assessed for the presence of cytopathic effect. (B) Cells were then treated with XTT and 3 h post treatment absorbances were read at 450 nM. Cell viability was determined, the mean and standard error of the mean were calculated from three separate experiments. (C) Cells were fixed and analyzed by fluorescent microscopy. Monoclonal antibodies against the NS1 protein were used to identify 1918-infected cells. DAPI stain was used to visualize each cell's nucleus.

developmental disorders, cell cycle, molecular transport, and cellular development (Fig. 3B; Supplementary Fig. S1). There were large numbers of proteins whose quantities changed when comparing 5 hpi pathways to 24 hpi pathways. For example, LBR was up-regulated at both 5 and 24 hpi but SMAD2 (and many other pathway members) were unaffected at 5 hpi and significantly down-regulated at 24 hpi (Table 1, Fig. 3B, Network 1). Similarly, most of the other top pathways had larger numbers of down-regulated proteins at the later time point. IPA identified numerous canonical pathways, diseases and biological functions that were significantly dysregulated, and/or that were predicted by *Z*-score analysis to be highly positively or negatively activated (Table 2). These observations were also complemented by DAVID analyses, which identified various proline dioxygenases and nucleotide binding activities (among others) as major up- and down-regulated molecular functions, and oxygen reduction and macromolecular complex organization and assembly as major biological processes (Fig. 4). The PI3K/mTOR/Akt canonical signaling pathway was one of the significantly affected ones (Table 2; Supplementary Fig. S2), supporting some of our recent observations about the role of this pathway in IAV replication [96]. To validate results obtained by mass spectrometry, we selected five differentially regulated proteins from Table 1, which targeted the various network and canonical pathways.These targeted proteins demonstrated clear changes in regulation, were detected in multiple experiments by mass spectrometry, and had reliable antibodies available for use. Using a similar experimental design as in the SILAC experiments, cells were infected at high multiplicity of infection (MOI) with 1918 virus (1918). The cells were fractionated into cytoplasmic and nuclear components and the expression levels of kinesin family 22 protein (KIF22), LBR, nuclear export factor 1 (NXF1), Nup205and Rab5b were assessed (Fig. 5). The non-biased SILAC screen demonstrated KIF22 up-regulation in the nuclear fraction at 5 hpi (Table 1) and that the protein was not detected in the cytoplasm or at later time points. Immunoblot analysis confirmed a statistically significant upregulation of KIF22 in the nucleus at 5 hpi but also demonstrated continued elevated expression at 24 hpi. In addition, KIF22 was detected in the cytoplasm although there was no statistically significant change observed with infection (Fig. 5B). The SILAC screen indicated LBR was up-regulated in the nucleus at both 5 and 24 hpi (Table 1) and similar trends were observed by immunoblot analysis (Fig. 5C). Although LBR was not detected in the cytoplasmic fractions by SILAC, immunoblot analysis, which is generally more sensitive, showed that LBR was also significantly up-regulated in the cytoplasm by 24 hpi (Fig. 5C). SILAC showed a 5-fold (2.2 $\log_2$-fold) decrease in NXF1 abundance in the nuclear fraction at 5 hpi and a no decrease at 24 hpi (Table 1) and immunoblot analysis demonstrated a slight decrease in NXF1 nuclear protein expression at 5 hpi and then a slight up-regulation at 24 hpi (Fig. 5D). While NXF1 was detected in

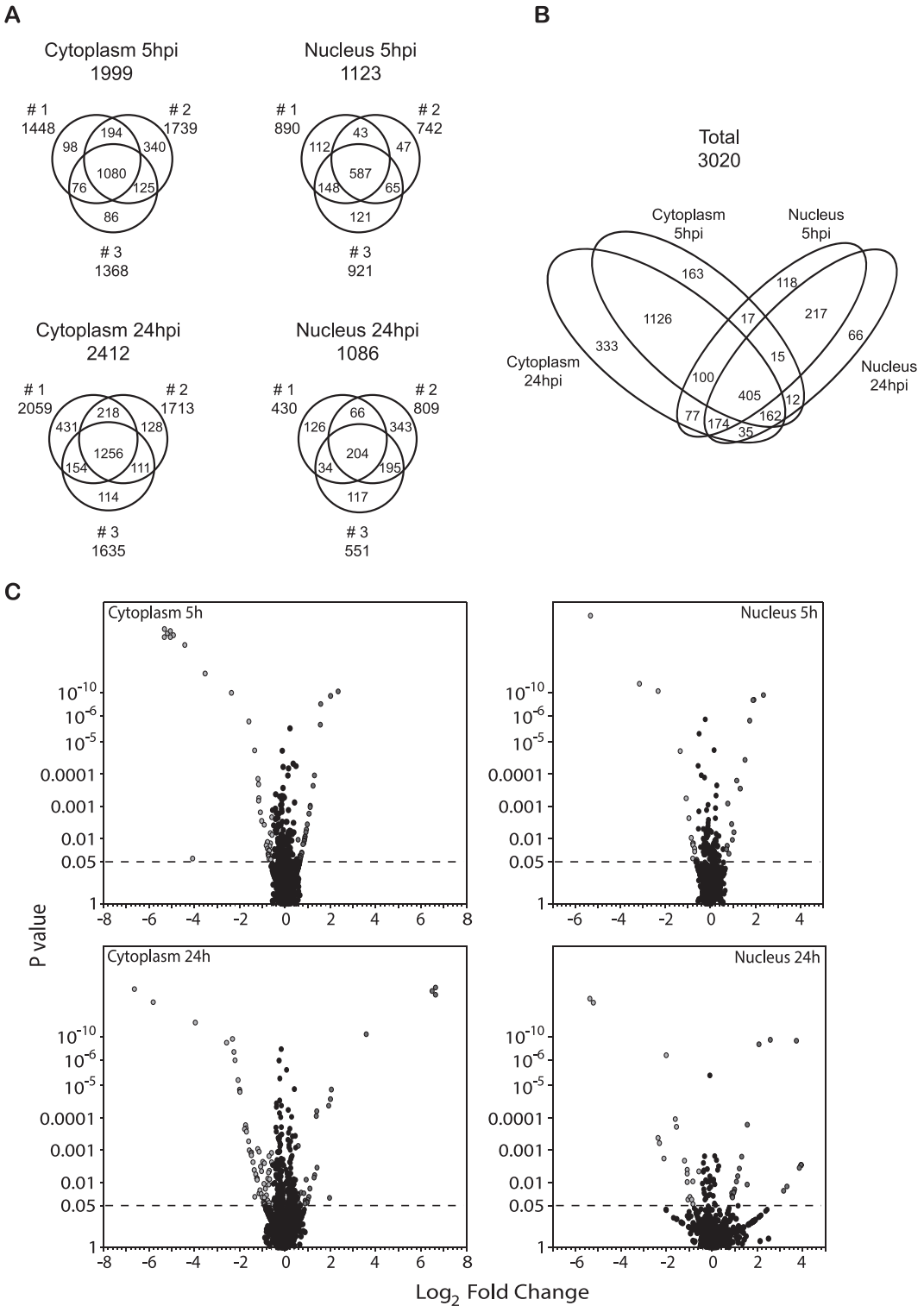

Fig. 2. Venn diagrams of protein distributions. A. Distribution and overlap of identified and measured proteins in each of the three replicates from each of the four indicated samples. The overall numbers of unique proteins in each of the 4 samples as well as in each replicate (#1, #2, and #3) are indicated. B. Distribution and overlap of measured proteins from both time points and from both sub-cellular fractions. C. Volcano plots of proteins' fold-change (expressed as Log_2 on X-axis) versus *p*-value (expressed on y-axis). Each protein is depicted by an individual circle. Proteins significantly up-regulated ≥1.5-fold (=0.585 Log_2) by infection, if measured multiple times, or significantly up-regulated ≥1.75-fold (=0.807 Log_2), if measured a single time, are indicated by red circles; proteins significantly down-regulated to ≤0.667-fold (=−0.585 Log_2), if measured multiple times, or significantly down-regulated to ≤0.5714-fold (=−0.807 Log_2), if measured a single time, are indicated by green circles,

SILAC cytoplasmic fractions, its expression level was not significantly altered due to infection.However, immunoblot analysis showed it slightly up-regulated at both time points (Fig. 5D). A lower level of NXF1 was expressed in the nucleus than in the cytoplasm, and infection resulted in reduced levels by 5 hpi that rebounded above the mock level by 24 hpi. Cytoplasmic Nup205 expression was similarly elevated when assessed by both SILAC and immunoblotting methods at 5 and 24 hpi (Table 1, Fig. 5E) but remained unchanged in the nucleus. Finally,

Table 1
A549 cell proteins affected by 1918 infection.

			Cytoplasm				Nucleus			
			5		24		5		24	
Accession	HGNC	Name	Count 1	I : M²	Count 1	I : M²	Count 1	I : M²	Count 1	I : M²
Up-regulated										
Detected more than once										
gi|72534670	PLAP	Phospholipase A2-activating protein	2	**2.98**	3	0.97	0		0	
gi|6005860	RL35	Ribosomal protein L35	2	**1.73**	1	1.67	2	1.19	3	0.98
gi|56090582	IRGQ	Immunity-related GTPase family, Q	2	**1.60**	3	0.80	0		0	
gi|59850762	UACA	Uveal autoantigen with coiled-coil domains and ankyrin repeats isoform 1	3	**1.58**	3	0.79	0		0	
gi|7706501	WBP11	WW domain binding protein 11	2	**1.56**	0		0		0	
gi|22538442	CATZ	Cathepsin Z preproprotein	2	**1.55**	2	1.24	0		0	
gi|18087829	ZC3HAV1L	Zinc finger CCCH-type, antiviral 1-like	2	**1.52**	0		0		0	
gi|221625487	IMPA1	Inositol(myo)-1(or 4)-monophosphatase 1 isoform 2	3	1.00	2	**12.02**	0		0	
gi|4506019	2ABA	Alpha isoform of regulatory subunit B55, protein phosphatase 2	2	1.00	3	**4.13**	0		0	
gi|4506371	RAB5B	RAB5B, member RAS oncogene family	0		2	**4.01**	1	0.72	0	
gi|20149498	FRIL	Ferritin, light polypeptide	1	1.34	2	**3.91**	0		0	
gi|4826852	ACPM	NADH dehydrogenase (ubiquinone) 1, alpha/beta subcomplex, 1, 8kDa	3	0.98	2	**2.66**	3	1.09	2	0.99
gi|57634534	NUP205	Nucleoporin 205kDa	1	**2.08**	2	**2.64**	0		0	
gi|156104864	ACOX3	Acyl-Coenzyme A oxidase 3 isoform a	0		2	**2.14**	0		0	
gi|57222565	PP2AB	Protein phosphatase 2, catalytic subunit, beta isoform	0		2	**1.97**	0		0	
gi|4506669	RLA1	Ribosomal protein P1 isoform 1	3	1.03	3	**1.97**	3	1.05	3	0.99
gi|6857824	IFT27	RAB, member of RAS oncogene family-like 4	0		2	**1.90**	0		0	
gi|4502989	COX7A2	Cytochrome c oxidase subunit VIIa polypeptide 2 (liver) precursor	0		2	**1.85**	3	1.12	2	1.01
gi|134142337	MRP1	ATP-binding cassette, sub-family C, member 1 isoform 1	0		2	**1.85**	1	0.87	1	1.13
gi|7657609	SC11A	SEC11-like 1	0		2	**1.84**	3	0.73	1	**4.20**
gi|7706481	CAB39	Calcium binding protein 39	1	1.00	2	**1.78**	0		0	
gi|19923475	TRM6	tRNA methyltransferase 6	0		2	**1.53**	0		0	
gi|66933016	IMDH2	Inosine monophosphate dehydrogenase 2	3	1.05	3	1.03	2	**3.35**	2	1.11
gi|153792590	HS90A	Heat shock 90kDa protein 1, alpha isoform 1	2	1.00	3	1.06	2	**2.50**	2	2.68
gi|37595752	LBR	Lamin B receptor	0		0		2	**1.92**	1	**2.93**
gi|16507237	GRP78	Heat shock 70kDa protein 5	3	1.02	3	1.18	3	**1.76**	3	0.92
gi|4504271	H2B1C	Histone cluster 1, H2bi	0		1	**0.01**	2	**1.70**	0	
gi|56676371	CPSF1	Cleavage and polyadenylation specific factor 1, 160kDa	0		0		1	0.90	2	**13.20**
gi|222352111	MK67I	MKI67 interacting nucleolar phosphoprotein	0		0		3	0.98	2	**1.84**
gi|4758790	NDUS5	NADH dehydrogenase (ubiquinone) Fe-S protein 5, 15kDa (NADH-coenzyme Q reductase)	0		1	1.12	2	0.97	2	**1.68**
Detected only once										
gi|4506901	SRSF3	Splicing factor, arginine/serine-rich 3	1	**5.07**	1	1.19	3	1.09	2	0.97
gi|156416005	COMD9	COMM domain containing 9 isoform 1	1	**4.02**	2	0.94	0		0	
gi|4502601	CBR3	Carbonyl reductase 3	1	**2.95**	1	0.63	0		0	
gi|134288884	SYEM	Glutamyl-tRNA synthetase 2	1	**2.46**	0		0		0	
gi|20149524	SPT5H	Suppressor of Ty 5 homolog isoform a	1	**2.36**	3	1.04	0		1	1.16

gi|21361358	STK25	Serine/threonine kinase 25	1	2.16	0		0		0	
gi|21361497	ACAD9	Acyl-Coenzyme A dehydrogenase family, member 9	1	2.15	3	1.15	0		0	
gi|187607323	EI2BD	Eukaryotic translation initiation factor 2B, subunit 4 delta isoform 1	1	1.97	0		0		0	
gi|40068481	SETD3	SET domain containing 3 isoform a	1	1.92	0		0		0	
gi|39725950	IPO11	Ran binding protein 11 isoform 2	1	1.89	0		0		0	
gi|63055059	SPD2B	SH3 and PX domains 2B	1	1.85	1	0.25	0		0	
gi|6005926	U2AF2	U2 (RNU2) small nuclear RNA auxiliary factor 2 isoform a	1	1.84	0		0		0	
gi|53729363	LRSM1	Leucine rich repeat and sterile alpha motif containing 1	1	1.83	1	0.87	0		0	
gi|6005786	MGLL	Monoglyceride lipase isoform 1	1	1.81	0		0		0	
gi|67089147	FDFT	Squalene synthase	1	1.80	3	0.61	0		0	
gi|61743967	CTBP1	C-terminal binding protein 1 isoform 2	1	1.78	2	0.99	0		0	
gi|31377806	PIGR	Polymeric immunoglobulin receptor precursor	0		1	100.00	0		0	
gi|7657387	CNOT3	CCR4-NOT transcription complex, subunit 3	1	1.41	1	100.00	0		0	
gi|4507261	STAT	Statherin isoform a	0		1	100.00	0		0	
gi|52630326	CHD3	Chromodomain helicase DNA binding protein 3 isoform 1	0		1	3.80	0		0	
gi|148728162	PTPRJ	Protein tyrosine phosphatase, receptor type, J isoform 1 precursor	0		1	2.60	1		0	
gi|17978479	VPS16	Vacuolar protein sorting 16 isoform 1	0		1	2.48	0		0	
gi|53793688	H32	Histone cluster 2, H3a	0		1	2.44	1	0.94	1	0.98
gi|6715600	GOGA4	Golgi autoantigen, golgin subfamily a, 4	0		1	1.91	0		0	
gi|74275350	TSPO	Translocator protein isoform PBR	0		0		1	61.66	1	1.34
gi|4758086	CSRP1	Cysteine and glycine-rich protein 1 isoform 1	3	0.97	3	0.95	1	5.11	0	
gi|21735621	MDHM	Mitochondrial malate dehydrogenase precursor	3	1.13	3	1.37	1	3.80	2	0.77
gi|4507677	ENPL	Heat shock protein 90kDa beta, member 1	3	1.06	3	1.14	1	3.70	3	2.09
gi|20070125	PDIA1	Prolyl 4-hydroxylase, beta subunit precursor	3	1.04	3	1.10	1	2.90	2	2.18
gi|6453818	KIF22	Kinesin family member 22	0		0		1	2.24	0	
gi|39652628	F120A	Oxidative stress-associated Src activator	3	0.92	3	0.89	1	2.06	1	0.91
gi|4885281	DHE3	Glutamate dehydrogenase 1	3	1.00	3	1.15	1	1.97	1	3.78
gi|19923667	RSAD2	Radical S-adenosyl methionine domain containing 2	0		0		0		1	15.22
gi|21361322	TBB4A	Tubulin, beta 4	0		0		0		1	15.22
gi|222136619	MX1	Myxovirus resistance protein 1	0		1		0		1	15.22
gi|4503535	IF4E	Eukaryotic translation initiation factor 4E isoform 1	0		1	0.71	0		1	15.22
gi|45359849	G3BP2	Ras-GTPase activating protein SH3 domain-binding protein 2 isoform a	3	1.03	3	0.86	0		1	15.22
gi|51599151	CPNS1	Calpain, small subunit 1	3	0.93	3	0.90	0		1	15.22
gi|55749932	DESM	Desmin	0		0		0		1	15.22
gi|91823262	ANXA8	Annexin A8	2	1.00	1	1.46	0		1	14.42
gi|63252913	CAPG	Gelsolin-like capping protein	3	0.95	3	1.11	0		1	9.86
gi|31542862	GRWD1	Glutamate-rich WD repeat containing 1	2	0.90	2	1.05	2	0.89	1	5.96
gi|4885487	MLF2	Myeloid leukemia factor 2	0		0		0		1	2.95
gi|14165270	RM13	Mitochondrial ribosomal protein L13	0		1		2	0.87	1	2.48
gi|4504269	H2B1H	Histone cluster 1, H2bh	0		0		0		1	2.20
gi|42491362	IKIP	IKK interacting protein isoform 2	0		0		2	0.90	1	2.12

Down-regulated

Detected more than once

gi|149999606	MOGS	Mannosyl-oligosaccharide glucosidase isoform 1	3	**0.05**	3	1.18	0		1	
gi|4507143	SNX3	Sorting nexin 3 isoform a	2	**0.06**	1	1.52	0		0	
gi|4507131	RUXF	Small nuclear ribonucleoprotein polypeptide F	2	**0.09**	0		3	1.06	1	0.99
gi|194578885	CALU	Calumenin isoform b precursor	3	**0.19**	1	1.20	0		1	3.58
gi|6677723	RFC5	Replication factor C 5 isoform 1	2	**0.45**	1	**2.07**	0		0	
gi|27436889	OFUT1	Protein O-fucosyltransferase 1 isoform 1 precursor	2	**0.47**	3	1.07	0		0	
gi|14589951	RPAB1	DNA directed RNA polymerase II polypeptide E	3	**0.53**	2	0.80	3	0.72	1	
gi|48255937	CD44	CD44 antigen isoform 2 precursor	2	**0.58**	3	0.77	1	1.11	0	
gi|34740329	ROA3	Heterogeneous nuclear ribonucleoprotein A3	2	**0.58**	3	1.45	3	1.06	3	0.98
gi|30581135	SMC1A	Structural maintenance of chromosomes 1A	2	**0.59**	3	1.01	3	0.91	1	0.94
gi|166795301	PCYOX	Prenylcysteine oxidase 1	2	**0.61**	3	1.04	0		0	
gi|58331268	ERC6L	Excision repair protein ERCC6-like	3	**0.61**	0		0		0	
gi|21040257	TRUB1	TruB pseudouridine (psi) synthase homolog 1	2	**0.62**	1	0.86	0		0	
gi|4507467	BGH3	Transforming growth factor, beta-induced, 68kDa precursor	3	**0.64**	3	0.62	1	**0.64**	0	
gi|114326552	MON2	MON2 homolog	3	**0.64**	3	0.84	0		0	
gi|148728166	HTAI2	HIV-1 Tat interactive protein 2, 30kDa isoform a	2	**0.65**	1	0.93	0		0	
gi|6005721	ERLN2	ER lipid raft associated 2 isoform 1	0		3	**0.06**	3	1.06	1	1.23
gi|208973246	DHPR	Quinoid dihydropteridine reductase	3	1.22	2	**0.20**	0		0	
gi|4757826	B2MG	Beta-2-microglobulin precursor	1	1.18	2	**0.29**	3	0.77	0	
gi|4557719	DNLI1	DNA ligase I	1	1.19	2	**0.31**	0		0	
gi|21264355	SMCE1	SWI/SNF-related matrix-associated actin-dependent regulator of chromatin e1	0		2	**0.34**	1	0.74	0	
gi|7657671	UBF1	Upstream binding transcription factor, RNA polymerase I isoform a	1		2	**0.36**	2	0.87	1	1.75
gi|4503165	CUL3	Cullin 3	3	0.96	3	**0.39**	0		0	
gi|63252893	P4HA2	Prolyl 4-hydroxylase, alpha II subunit isoform 2 precursor	2	0.86	3	**0.40**	0		0	
gi|5031887	LPP	LIM domain containing preferred translocation partner in lipoma	2	0.94	3	**0.45**	0		0	
gi|4758334	FADS2	Fatty acid desaturase 2	1		2	**0.45**	1	0.70	0	
gi|4557769	KIME	Mevalonate kinase	2	1.07	2	**0.50**	0		0	
gi|4504151	GRN	Granulin precursor	1	1.26	2	**0.51**	0		0	
gi|4506439	RBBP7	Retinoblastoma binding protein 7	3	1.04	3	**0.53**	1	0.90	0	
gi|5174511	SMAD2	Sma- and Mad-related protein 2 isoform 1	1	1.47	2	**0.53**	0		0	
gi|116734704	I2BP2	Interferon regulatory factor 2 binding protein 2 isoform A	3	1.04	2	**0.54**	0		0	
gi|72534748	MTNA	Translation initiation factor eIF-2B subunit alpha/beta/delta-like protein isoform 1	2	0.73	3	**0.55**	0		0	
gi|156631005	PSMD8	Proteasome 26S non-ATPase subunit 8	0		2	**0.57**	0		0	
gi|118150660	ZC3HF	Erythropoietin 4 immediate early response	2	0.98	2	**0.57**	0		0	
gi|4504619	IBP7	Insulin-like growth factor binding protein 7	2	0.81	3	**0.59**	0		1	**2.23**
gi|46249388	SERB	Phosphoserine phosphatase	3	1.12	2	**0.59**	0		0	
gi|4757718	ACL6A	Actin-like 6A isoform 1	0		2	**0.61**	3	0.94	1	1.21
gi|4503243	CP51A	Cytochrome P450, family 51, subfamily A, polypeptide 1 isoform 1	0		3	**0.62**	0		0	

gi|22547138	RM04	Mitochondrial ribosomal protein L4 isoform a	0		1	1.16	2	**0.11**	1	**2.31**
gi|15487670	NXF1	Nuclear RNA export factor 1 isoform 1	1	1.12	0		2	**0.20**	1	0.96
gi|38016127	RBM34	RNA binding motif protein 34	0		0		3	**0.55**	2	0.95
gi|29789090	RCC2	Regulator of chromosome condensation 2	3	0.95	3	0.82	3	**0.58**	0	
gi|24430146	NUP153	Nucleoporin 153kDa	0		0		2	**0.58**	0	
gi|41406064	MYH10	Myosin, heavy polypeptide 10, non-muscle	3	1.03	3	0.92	2	**0.61**	2	0.98
gi|4885409	VIGLN	High density lipoprotein binding protein	3	0.92	3	0.81	3	**0.62**	2	1.22
gi|115430235	UHRF1	Ubiquitin-like with PHD and ring finger domains 1 isoform 1	0		0		3	**0.64**	1	0.91
gi|7657581	CMC2	Solute carrier family 25, member 13 isoform 2	0		0		2	**0.66**	1	1.04
gi|32454741	SERPH	Serine (or cysteine) proteinase inhibitor, clade H, member 1 precursor	3	0.95	3	1.02	0		2	**0.31**
gi|7705706	RS27L	Ribosomal protein S27-like	2	1.02	3	1.02	0		2	**0.47**
gi|62912457	P5CS	Pyrroline-5-carboxylate synthetase isoform 2	3	0.80	3	1.06	2	0.92	2	**0.56**
Detected only once										
gi|10863895	TYB10	Thymosin, beta 10	1	**0.03**	1	0.59	0		0	
gi|149944496	UBXN7	UBX domain containing 7	1	**0.03**	2	0.58	0		0	
gi|157694494	MBB1A	MYB binding protein 1a isoform 1	1	**0.03**	3	1.06	2	0.93	2	1.01
gi|209969695	ISOC2	Isochorismatase domain containing 2 isoform 1	1	**0.03**	1	1.08	0		0	
gi|29553970	H2AJ	H2A histone family, member J	1	**0.03**	0		0		0	
gi|91208423	TRIP6	Thyroid receptor-interacting protein 6	1	**0.03**	0		0		0	
gi|14149680	ESYT1	Extended synaptotagmin-like protein 1	1	**0.33**	3	1.14	2	0.97	0	
gi|13375746	CF211	Hypothetical protein LOC79624	1	**0.39**	0		0		0	
gi|223633935	CJ047	Hypothetical protein LOC254427	1	**0.44**	0		0		0	
gi|21361380	SNF8	EAP30 subunit of ELL complex	1	**0.45**	0		0		0	
gi|19923750	RAB3B	RAB3B, member RAS oncogene family	1	**0.45**	1	1.60	0		0	
gi|22035672	TRXR2	Thioredoxin reductase 2 precursor	1	**0.49**	0		0		0	
gi|5453898	PIN1	Protein (peptidyl-prolyl cis/trans isomerase) NIMA-interacting 1	0		1	**0.02**	0		0	
gi|4504277	H2B2E	Histone cluster 2, H2be	0		1	**0.17**	2	1.38	1	0.53
gi|42716297	CLU	Clusterin isoform 1	0		1	**0.21**	0		0	
gi|52630440	FKBP8	FK506-binding protein 8	0		1	**0.22**	0		0	
gi|24234683	UBP11	Ubiquitin specific peptidase 11	0		1	**0.24**	0		0	
gi|189027129	PDE12	Phosphodiesterase 12	0		1	**0.25**	0		0	
gi|15011974	ARHG2	Rho/rac guanine nucleotide exchange factor 2	0		1	**0.25**	0		0	
gi|4502741	CDK6	Cyclin-dependent kinase 6	1	1.28	1	**0.30**	0		0	
gi|62865635	ERG1	Squalene epoxidase	0		1	**0.30**	0		0	
gi|116734706	I2BP2	Interferon regulatory factor 2 binding protein 2 isoform B	0		1	**0.33**	0		0	
gi|21624639	CSNK1A1L	Casein kinase 1, alpha 1-like	0		1	**0.35**	0		0	
gi|21735598	PDCD4	Programmed cell death 4 isoform 2	0		1	**0.36**	0		0	
gi|7661890	SNX17	Sorting nexin 17	2	0.91	1	**0.38**	0		0	
gi|13489073	EGLN1	Egl nine homolog 1	1	0.90	1	**0.41**	0		0	
gi|34577049	DYST	Dystonin isoform 1eA precursor	0		1	**0.42**	0		0	
gi|148612809	WNK1	WNK lysine deficient protein kinase 1	3	1.01	1	**0.42**	0		0	
gi|65786661	BTBDB	BTB (POZ) domain containing 11 isoform a	3	0.93	1	**0.42**	0		0	
gi|55770850	CP24A	Cytochrome P450 family 24 subfamily A polypeptide 1 isoform 1 precursor	2	1.14	1	**0.43**	0		0	

gi|73765546	UB2V1	Ubiquitin-conjugating enzyme E2 variant 1 isoform d	1	1.09	1	**0.43**	0		0	
gi|4758332	ACSL4	Acyl-CoA synthetase long-chain family member 4 isoform 1	2	0.98	1	**0.48**	0		0	
gi|4758220	FA50A	XAP-5 protein	3	0.87	1	**0.49**	0		0	
gi|205360838	DNJA3	DnaJ (Hsp40) homolog, subfamily A, member 3 isoform 1	0		1	**0.53**	0		0	
gi|187281616	NDUS7	NADH-ubiquinone oxidoreductase Fe-S protein 7 precursor	0		0		1	**0.03**	1	**0.54**
gi|170296790	TRY3	Mesotrypsin isoform 1 preproprotein	0		0		1	**0.39**	0	
gi|47519616	TPM2	Tropomyosin 2 (beta) isoform 2	3	1.01	3	0.93	1	**0.47**	1	0.96
gi|5454122	TIM23	Translocase of inner mitochondrial membrane 23 (yeast) homolog	0		0		1	**0.52**	0	
gi|14589889	CADH2	Cadherin 2, type 1 preproprotein	0		2	0.86	3	1.14	1	**0.02**
gi|154354962	IMMT	Inner membrane protein, mitochondrial isoform 2	0		0		0		1	**0.02**
gi|22538467	PSB4	Proteasome beta 4 subunit	3	1.11	3	1.12	0		1	**0.19**
gi|70995422	NQO1	NAD(P)H menadione oxidoreductase 1, dioxin-inducible isoform c	0		0		0		1	**0.20**
gi|5453543	AK1C1	Aldo-keto reductase family 1, member C1	0		1	0.95	0		1	**0.23**
gi|47132557	FINC	Fibronectin 1 isoform 1 preproprotein	0		0		2	1.31	1	**0.25**
gi|4504505	DHB4	Hydroxysteroid (17-beta) dehydrogenase 4	3	1.04	3	1.23	0		1	**0.33**
gi|16332372	CD11B	Cell division cycle 2-like 1 (PITSLRE proteins) isoform 9	0		0		0		1	**0.34**

Significance assumed if measured ≥2 times and up-regulated ≥1.5-fold, or if down-regulated to ≤0.667-fold compared to mock; or if measured only once and up-regulated ≥1.75-fold, or if down-regulated to ≤0.571-fold compared to mock, as determined by *t*-test or z-score analysis and as described in reference #19.
[1]The number of replicates from which protein quantities were measured.
[2]Infected: mock-infected ratio.
[3]**Red** highlight indicates significant up-regulation; **green** indicates significant down-regulation. Proteins arranged top-to-bottom in each half of table from most regulated to least regulated and sorted from Cytoplasm 5 h - Nucleus 24 h.

SILAC showed Rab5b up-regulation in the cytoplasmic fraction at 24 hpi, although it was not detected at the earlier time point and immunoblot showed significant up-regulation of Rab5b at both 5 and 24 hpi (Fig. 5F). Rab5b was not detected in nuclear fractions by mass spectrometry (Table 1), and was barely detectable by immunoblotting. Thus, while not perfect correlation, there was general consistency between the non-biased SILAC method and the more targeted and more sensitive immunoblotting method. Minor differences in degree or direction of measured regulation might be attributable to inherent differences in sampling (partially degraded proteins would not be measured by immunoblot but their peptides would be detected by MS) or by inherent differences in the sensitivity of each method.

3.2. Differential Host Responses Are Induced by Different IAV Strains

We have previously described host proteomic responses to infection by the lab and mouse-adapted IAV strain A/Puerto Rico/8/34 (H1N1) [12] and we also previously showed that highly pathogenic avian influenza virus strains H5N1 and H7N9 induced more profound alterations than the seasonal or 2009 pandemic IAV H1N1 strains [81]. To extend our findings with the 1918 virus to other influenza strains, we then used immunoblotting to determine whether KIF22, LBR, NXF1, Nup205 and Rab5b were similarly or differentially induced or repressed by representatives of each of the other virus subtypes. As a control, the 1918 virus was used to confirm our previous findings, and we included three additional H1N1 strains: A/Mexico/InDRE4487/2009 (Mx10), a 2009 pandemic H1N1 isolate from a patient in Mexico; A/Canada/RV733/2007 (RV733), a seasonal strain from 2007 that was isolated from an infected patient in Canada; and A/USSR/90/1977 (U77), a patient isolate collected during the re-emergence of the H1N1 subtype in 1977. We also included two avian-origin viruses associated with highly pathogenic infection in humans: A/Vietnam/1203/2004 (V1203), a H5N1 virus isolated from a patient from Vietnam in 2004; and A/Anhui/1/2013 (Anh2013), a H7N9 virus isolated from a patient in China in 2013. A549 cells were infected with the abovementioned panel of viruses at an MOI of 7. Total cell lysates were collected 24 hpi and analyzed by immunoblotting. The 1918-infected cells demonstrated similar protein expression patterns (Fig. 6) as seen in the previous experiment (Fig. 5). There were a few minor changes in expression levels of the five proteins but that would be expected when comparing fractionated samples (Fig. 5) to total cell lysates (Fig. 6). The human H1N1 strains 1918, Mx10, RV733, and U77; and avian-origin H7N9 (Anh2013) viruses all up-regulated expression of KIF22 to similar levels upon infection. Interestingly, there was statistically significant down-regulation of KIF22 expression when cells were infected with V1203 (Fig. 6A, $p < 0.01$). There was a statistically significant difference between the LBR expression profiles of 1918-infected cells compared to the other strains that were tested. 1918-infected cells had elevated levels of LBR at 24 hpi, while the other tested strains all showed an inhibition of LBR expression (Fig. 6B, $p < 0.01$). NXF1 expression was mildly elevated in cells infected with the human H1N1 viruses or the avian Anh2013; however, when infected with V1203 there was a significant inhibition of NXF1 expression at 24 hpi (Fig. 6C, $p < 0.001$). While there was no statistically significant difference in the expression patterns of Nup205 between cells infected with this panel of viruses, U77 and V1203 tended to trend lower when Nup205 expression was assessed (Fig. 6D). Finally, Rab5b expression profiles had a statistically significant difference between 1918-infected cells and the other strains tested. Infection with 1918 caused the highest increase in Rab5b expression, Mx10, U77, RV733 and Anh2013 caused mild elevation, while

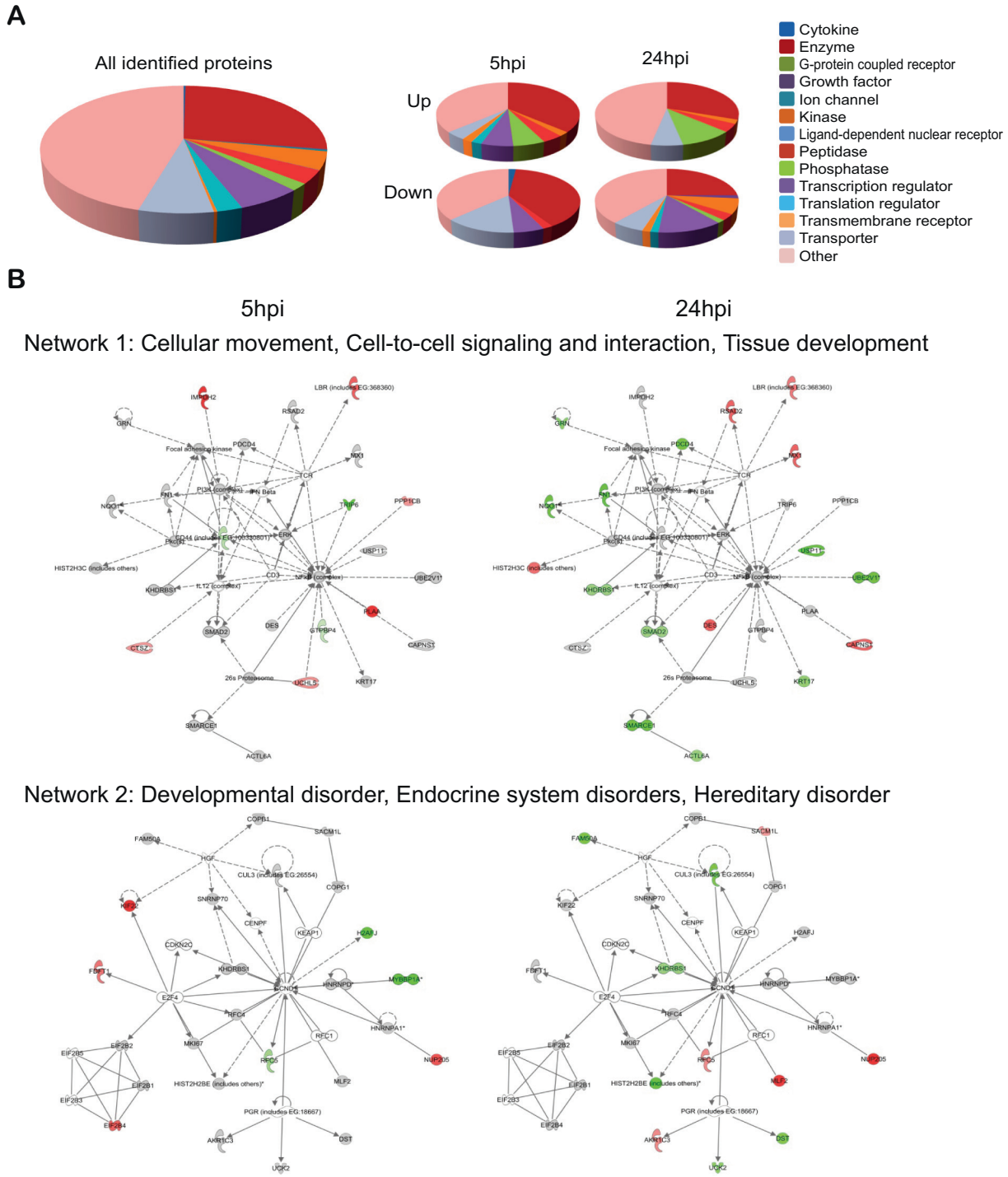

Fig. 3. Molecular pathways of regulated proteins. Proteins and their levels of regulation were imported into the Ingenuity Pathways Analysis (IPA®) tool and interacting pathways were constructed. A, Ontological classifications of all measured proteins (Total) as well as those significantly up- and down-regulated at each of 5 and 24 hpi. B, The top 2 networks, identified at 95% confidence and each of which contained 14 or more "focus" molecules (molecules significantly up- or down-regulated), with pathway names indicated. Three additional high-scoring networks, each also identified at 95% confidence and each of which contained 14 or more "focus" molecules are shown in Supplementary Fig. S1. Solid lines: direct known interactions; dashed lines: suspected or indirect interactions. Red: significantly up-regulated proteins at the indicated time point; pink: moderately up-regulated proteins; grey: proteins identified but not significantly regulated; light green: moderately down-regulated proteins; dark green: significantly down-regulated proteins; white: proteins known to be in network, but not identified in our study.

most strikingly infection with V1203 resulted in a decrease in Rab5b expression (Fig. 6E, $p < 0.001$).

Our lab focuses on identifying changes in the host response caused by influenza virus infections for a variety of different strains to better delineate viral life cycles and features of pathogenesis [12,48,81,96]. To provide more evidence that the changes we observed in protein expression profiles correlated with a pathway response required for influenza infection/propagation, we looked at whether infection altered signaling pathways that are linked to expression of the proteins assessed in this study. Previously, utilizing a lab-adapted A/Puerto Rico/8/34 (H1N1) (PR8) strain, we identified changes in apoptosis and autophagy and the PI3K/Akt/mTOR regulatory pathway was suggested

Table 2
Most significant canonical pathways, diseases and biological functions[a].

	$-\text{Log}_{10}$ p-value	Activation Z score
Top canonical pathways		
EIF2 signaling	64.2	↑[b] **3.6927**
Regulation of eIF4 and p70S6K signaling	34.1	0.6882
Mitochondrial dysfunction	28.3	
Protein ubiquitination pPathway	27.5	
mTOR signaling	24	↑ 0.9285
Oxidative phosphorylation	21.9	
Remodeling of epithelial adherens junctions	20.3	−0.6882
tRNA charging	16.1	
Integrin signaling	14.8	0.1280
Actin cytoskeleton signaling	13.3	−0.7620
Caveolar-mediated endocytosis signaling	12	
NRF2-mediated oxidative stress response	11.9	−0.3651
14-3-3-mediated signaling	6.33	↑ **2.1213**
HIPPO signaling	6.29	↓ **−2.0000**
Hypoxia signaling in the cardiovascular system	5.12	↑ **2.0000**
Ephrin B signaling	4.84	↓ **−2.3238**
Cell cycle: G2/M DNA damage checkpoint regulation	4.57	↑ **2.3094**
ERK5 signaling	2.26	↑ **2.6726**
Top diseases & bio functions		
Cell death and survival	60.97	↓ **−2.2470**
Cancer, cell death and survival, organismal injury and abnormalities, tumor morphology	55.97	↓ **−2.8300**
RNA post-transcriptional modification	54.57	−0.1250
Infectious diseases	50.88	↓ **−2.2170**
Cellular growth and proliferation	49.22	−0.3250
Protein synthesis	47.74	−0.7560
RNA post-transcriptional modification	35.82	−0.3440
Cell cycle	7.96	↓ **−2.6300**
Cell-to-cell signaling and interaction	6.99	↓ **−2.2720**

[a] As determined by Ingenuity Pathway Analysis®.
[b] Up-arrows indicate pathway or function positive activation; down-arrows indicate negative activation. Bolded *Z*-score values indicate significance > +1.96 or < 1.96 sigma.

to play a role [96]. Our data using the 1918 strain also confirmed the PI3K/Akt/mTOR pathway was affected during infection (Supplementary Fig. S2). Furthermore, we noted that four of the five proteins (excluding KIF22) we analyzed interact with the PI3K/AKT/mTOR signaling cascade, a pathway that is responsible for regulating the cell cycle and cellular survival. PI3K, AKT and mTOR are the central junctions of this pathway. Cell surface receptor tyrosine kinases, (RTK) respond to various growth factors, cytokines and hormones and activate phosphatidylinositol 3-kinase (PI3K) which in turn promotes production of phosphatidylinositol 3,4,5-trisphosphate (PIP3).PIP3 recruits and activates AKT and mTOR is activated by the activities of PI3K and AKT. AKT and mTOR exert a variety of upstream and downstream effects such as control of protein transcription and translation, autophagy, lipid synthesis and mitochondrial function (Fig. 7). We compared the phosphorylation states of a variety of proteins within this pathway between mock-infected cells and cells infected with 1918, Mx10, RV733, V1203 and Anh2013 as previously described. Cells infected with 1918 showed reduced phosphorylation levels of proteins within this pathway at 5 hpi (Fig. 8A). By 24 hpi many of the proteins had returned to normal phosphorylation levels, specifically AKT and mTOR (Fig. 8B). Mx10 demonstrated very similar results to those of the 1918 group. At 5 hpi, Mx10-infected cells demonstrated an overall decline in phosphorylation of proteins from the AKT/mTOR pathway (Fig. 8B), and by 24 hpi the phosphorylation levels had almost completely returned to steady state levels observed in mock-infected samples (Fig. 8B). When cells were infected with a seasonal H1N1 strain, RV733, a few proteins from the AKT/mTOR pathway had reduced phosphorylation at 5 hpi and by 24 hpi almost the entire pathway was dephosphorylated, demonstrating a slower inhibition of the pathway (Fig. 8). It is not known whether the pathway returned to steady state levels as occurred for the other H1N1viruses tested after 24 h. Interestingly, the two tested avian viruses (V1203 and Anh2013) behaved differently.At 5 hpi both viruses exhibited decreased phosphorylation of a number of proteins in the AKT/mTOR pathway, as seen with the H1N1 viruses; however, a notable distinction between the avian and H1N1 strains was the observed early phosphorylation of AKT and either GSK3α or GSK3β depending on the virus (Fig. 8A). GSK3α and GSK3β play redundant roles in the pathway; they both are phosphorylated by AKT, and in turn their activity is inhibited. Therefore, an increase in AKT activation would correlate with an increase in phosphorylation of either GSK3 species. By 24 hpi, V1203-infected cells demonstrated further and significant decrease in phosphorylation of almost all of the proteins assessed, including GSKα, GSKβ and AKT, while several proteins in the Anh2013-infected cells returned to steady state levels with a few exceptions (Fig. 8B).

From our previous data, we saw that the two pandemic viruses, 1918 and Mx10, responded similarly; at 5 hpi there was a general depression of the AKT/mTOR pathway followed by a return to steady state levels by 24 hpi. V1203 and RV733 also demonstrated a depression of the AKT/mTOR pathway but it was delayed compared to 1918 and Mx10, while Anh2013 appeared to alter only the phosphorylation state of a few proteins in the pathway and an overall depression of the pathway was not observed at any time point. This outcome suggested that influenza virus infection may be selectively influencing the pathway to promote viral replication. Focusing on the role of mTOR, we used rapamycin, an inhibitor that specifically targets the mTORC1 complex. Here we assessed whether the inhibition of mTORC1 would affect influenza virus replication. Cells were infected with 1918, Mx10, RV733, V1203 or Anh2013, treated with rapamycin for either 5 or 24 h and viral replication was assessed at 48 hpi. Mx10, RV733, V1203 and Anh2013 virus replication were unaffected by treatment with rapamycin; however, 1918 replication was severely impaired by treatment with rapamycin, regardless of the time of treatment, suggesting a requirement for mTORC1 activity in early replication events of the 1918 virus (Fig. 9). A striking difference in the replication of the 1918 virus and the other viruses evaluated is that the 1918 virus replicates to at least 2–3 $\log_{10}$ higher titer when rapamycin is absent or at low, non-inhibitory concentrations.Following treatment at doses in the range of 1–10 nM, replication of the 1918 virus was reduced to levels that are similar to those observed with viruses that are not sensitive to rapamycin.This outcome suggests that the capacity of the 1918 virus to grow to significantly higher titers in A549 cells, compared to the other viruses, is dependent on the activity of mTOR, most probably in the context of its role in the mTORC1 complex.

4. Discussion

A number of genome-wide RNAi screens, mRNA microarray screens and yeast 2-hybid assays have defined cellular networks that are required for, or manipulated by, influenza infection. These studies have identified >1400 protein targets that may be worth further analysis [92]. The majority of these studies were performed with less pathogenic influenza virus strains and there was very little overlap between most studies. Because viral infection leads to both qualitative and quantitative effects on host gene expression and function, we have complemented these previous studies by performing quantitative proteomic assessments of influenza infections to further define the effects of influenza virus infection on host functions. Our earlier studies focused on quantitative analyses of host protein responses to the mouse-adapted and attenuated PR8 strain in both cultured A549 [12] and primary bronchotrachial cells [48] and on high-pathogenic avian virus strains in A549 cells [81].

We assessed changes in the host's global protein response after 1918 influenza virus infection by mass spectrometry. A previous study using microarray technology indicated the presence of a strong inflammatory cytokine/chemokine response but a diminished downstream antiviral response in non-human primates infected with 1918 [47]. Interestingly, using mass spectrometry, we identified a small proportion of cytokines

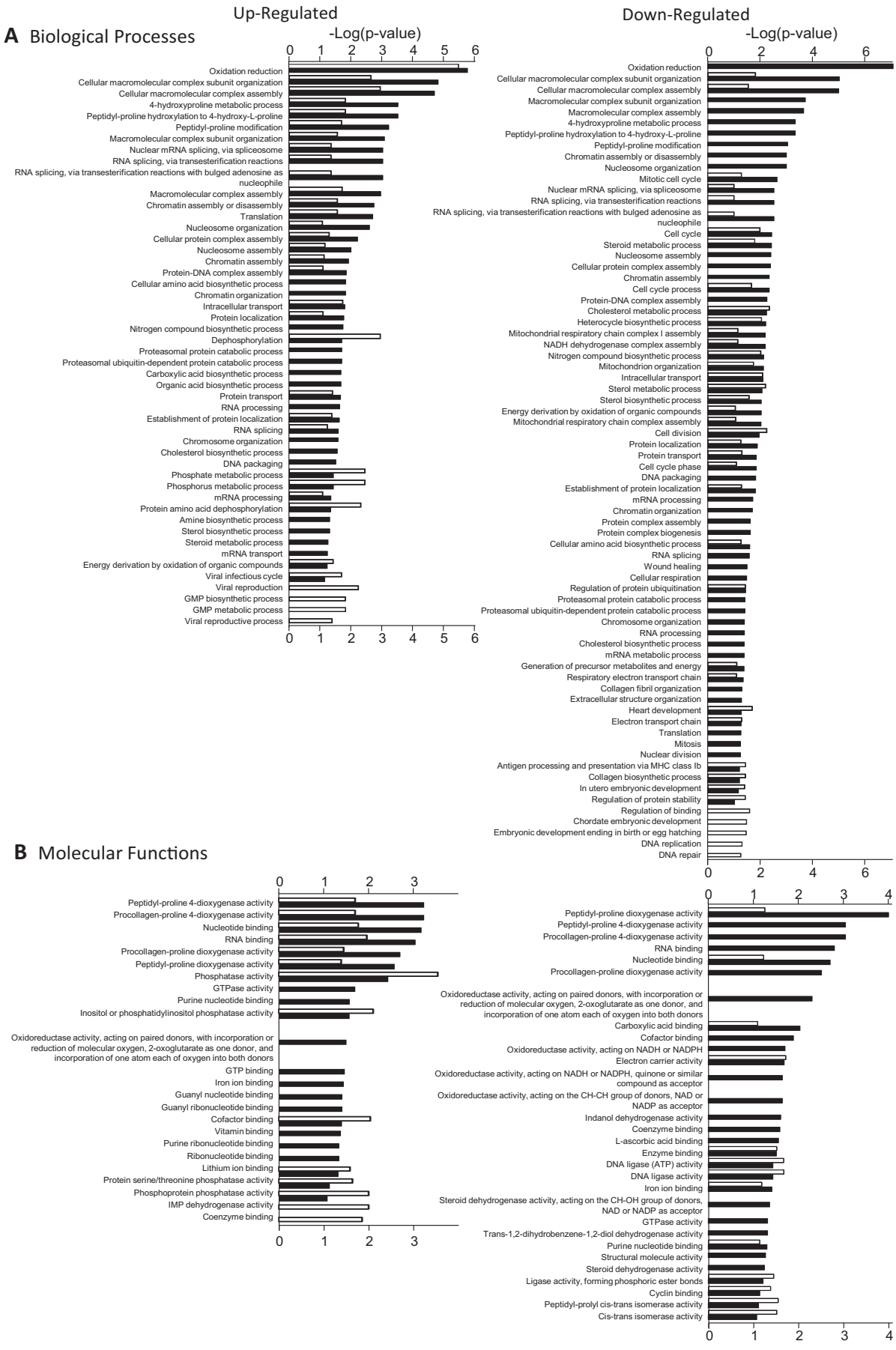
A Biological Processes
Up-Regulated
-Log(p-value)
0 1 2 3 4 5 6
Oxidation reduction
Cellular macromolecular complex subunit organization
Cellular macromolecular complex assembly
4-hydroxyproline metabolic process
Peptidyl-proline hydroxylation to 4-hydroxy-L-proline
Peptidyl-proline modification
Macromolecular complex subunit organization
Nuclear mRNA splicing, via spliceosome
RNA splicing, via transesterification reactions
RNA splicing, via transesterification reactions with bulged adenosine as nucleophile
Macromolecular complex assembly
Chromatin assembly or disassembly
Translation
Nucleosome organization
Cellular protein complex assembly
Nucleosome assembly
Chromatin assembly
Protein-DNA complex assembly
Cellular amino acid biosynthetic process
Chromatin organization
Intracellular transport
Protein localization
Nitrogen compound biosynthetic process
Dephosphorylation
Proteasomal protein catabolic process
Proteasomal ubiquitin-dependent protein catabolic process
Carboxylic acid biosynthetic process
Organic acid biosynthetic process
Protein transport
RNA processing
Establishment of protein localization
RNA splicing
Chromosome organization
Cholesterol biosynthetic process
DNA packaging
Phosphate metabolic process
Phosphorus metabolic process
mRNA processing
Protein amino acid dephosphorylation
Amine biosynthetic process
Sterol biosynthetic process
Steroid metabolic process
mRNA transport
Energy derivation by oxidation of organic compounds
Viral infectious cycle
Viral reproduction
GMP biosynthetic process
GMP metabolic process
Viral reproductive process
Down-Regulated
-Log(p-value)
0 2 4 6
Oxidation reduction
Cellular macromolecular complex subunit organization
Cellular macromolecular complex assembly
Macromolecular complex subunit organization
Macromolecular complex assembly
4-hydroxyproline metabolic process
Peptidyl-proline hydroxylation to 4-hydroxy-L-proline
Peptidyl-proline modification
Chromatin assembly or disassembly
Nucleosome organization
Mitotic cell cycle
Nuclear mRNA splicing, via spliceosome
RNA splicing, via transesterification reactions
RNA splicing, via transesterification reactions with bulged adenosine as nucleophile
Cell cycle
Steroid metabolic process
Nucleosome assembly
Cellular protein complex assembly
Chromatin assembly
Cell cycle process
Protein-DNA complex assembly
Cholesterol metabolic process
Heterocycle biosynthetic process
Mitochondrial respiratory chain complex I assembly
NADH dehydrogenase complex assembly
Nitrogen compound biosynthetic process
Mitochondrion organization
Intracellular transport
Sterol metabolic process
Sterol biosynthetic process
Energy derivation by oxidation of organic compounds
Mitochondrial respiratory chain complex assembly
Cell division
Protein localization
Protein transport
Cell cycle phase
DNA packaging
Establishment of protein localization
mRNA processing
Chromatin organization
Protein complex assembly
Protein complex biogenesis
Cellular amino acid biosynthetic process
RNA splicing
Wound healing
Cellular respiration
Regulation of protein ubiquitination
Proteasomal protein catabolic process
Proteasomal ubiquitin-dependent protein catabolic process
Chromosome organization
RNA processing
Cholesterol biosynthetic process
mRNA metabolic process
Generation of precursor metabolites and energy
Respiratory electron transport chain
Collagen fibril organization
Extracellular structure organization
Heart development
Electron transport chain
Translation
Mitosis
Nuclear division
Antigen processing and presentation via MHC class Ib
Collagen biosynthetic process
In utero embryonic development
Regulation of protein stability
Regulation of binding
Chordate embryonic development
Embryonic development ending in birth or egg hatching
DNA replication
DNA repair
B Molecular Functions
0 1 2 3
Peptidyl-proline 4-dioxygenase activity
Procollagen-proline 4-dioxygenase activity
Nucleotide binding
RNA binding
Procollagen-proline dioxygenase activity
Peptidyl-proline dioxygenase activity
Phosphatase activity
GTPase activity
Purine nucleotide binding
Inositol or phosphatidylinositol phosphatase activity
Oxidoreductase activity, acting on paired donors, with incorporation or reduction of molecular oxygen, 2-oxoglutarate as one donor, and incorporation of one atom each of oxygen into both donors
GTP binding
Iron ion binding
Guanyl nucleotide binding
Guanyl ribonucleotide binding
Cofactor binding
Vitamin binding
Purine ribonucleotide binding
Ribonucleotide binding
Lithium ion binding
Protein serine/threonine phosphatase activity
Phosphoprotein phosphatase activity
IMP dehydrogenase activity
Coenzyme binding
0 1 2 3 4
Peptidyl-proline dioxygenase activity
Peptidyl-proline 4-dioxygenase activity
Procollagen-proline 4-dioxygenase activity
RNA binding
Nucleotide binding
Procollagen-proline dioxygenase activity
Oxidoreductase activity, acting on paired donors, with incorporation or reduction of molecular oxygen, 2-oxoglutarate as one donor, and incorporation of one atom each of oxygen into both donors
Carboxylic acid binding
Cofactor binding
Oxidoreductase activity, acting on NADH or NADPH
Electron carrier activity
Oxidoreductase activity, acting on NADH or NADPH, quinone or similar compound as acceptor
Oxidoreductase activity, acting on the CH-CH group of donors, NAD or NADP as acceptor
Indanol dehydrogenase activity
Coenzyme binding
L-ascorbic acid binding
Enzyme binding
DNA ligase (ATP) activity
DNA ligase activity
Iron ion binding
Steroid dehydrogenase activity, acting on the CH-OH group of donors, NAD or NADP as acceptor
GTPase activity
Trans-1,2-dihydrobenzene-1,2-diol dehydrogenase activity
Purine nucleotide binding
Structural molecule activity
Steroid dehydrogenase activity
Ligase activity, forming phosphoric ester bonds
Cyclin binding
Peptidyl-prolyl cis-trans isomerase activity
Cis-trans isomerase activity

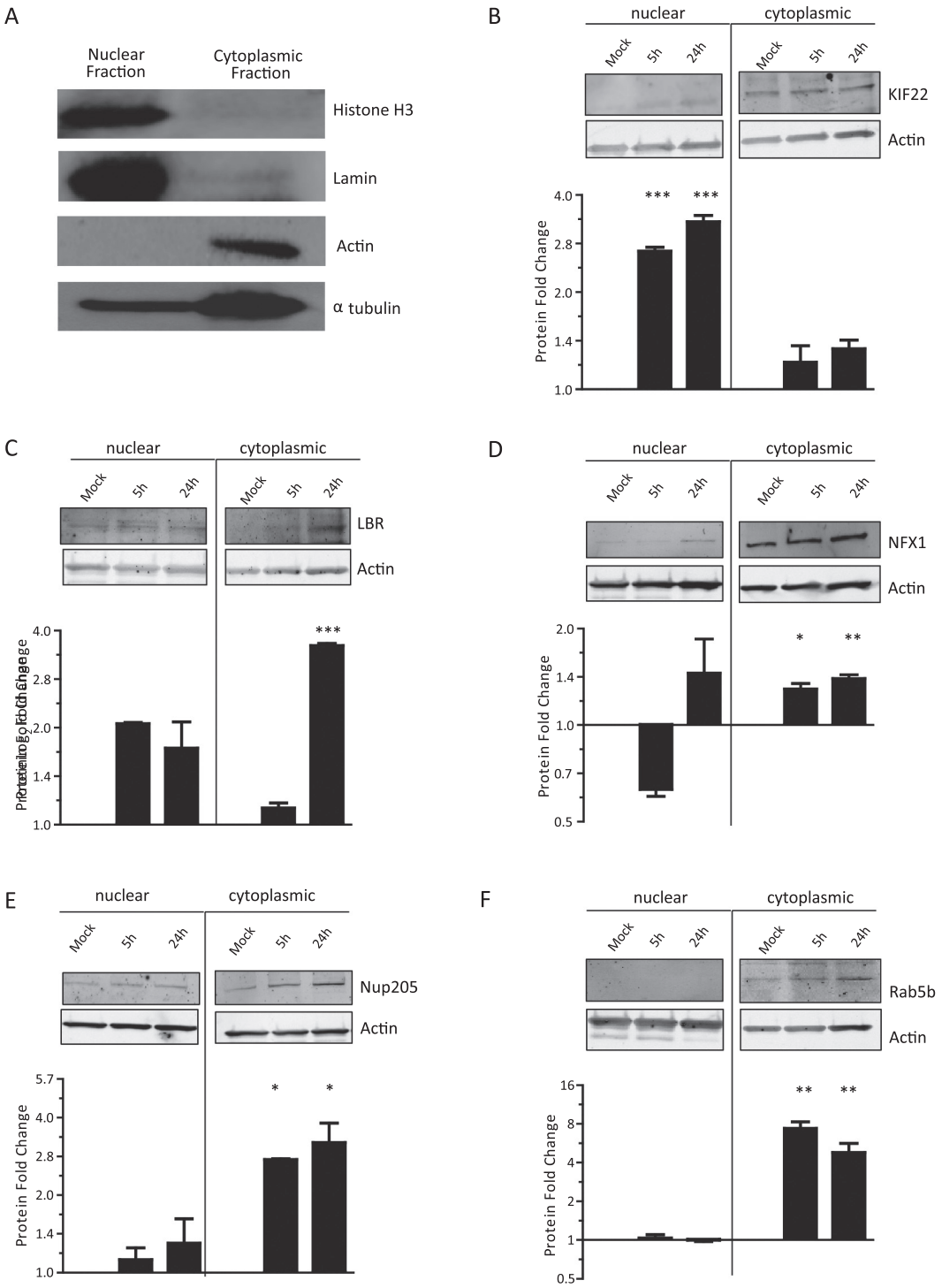

Fig. 5. Host protein expression profiles of nuclear and cytoplasmic fractions from 1918 infected cells. (A) Cells were fractionated and separated into nuclear and cytoplasmic fractions. Immunoblot analysis was conducted to ensure fractionation was complete. Histone H3 is found in the nucleus, Lamin is located in the nuclear envelope, actin is present in the cytoplasm, and α tubulin is situated in both the nucleus and cytoplasm. (B-F) A549 cells were infected with 1918 at an MOI of 7 and harvested at 5 and 24 h post-infection. Cells were fractionated and analyzed by immunoblot for specific proteins identified from the mass spectrometry analysis. Protein expression was quantified by densitometry and normalized to the expression of actin. The fold increase in protein expression was determined by comparing mock and infected samples. The means and standard error of the means were calculated from three separate protein expression experiments. A one-way Anova with a Bonferroni post-test was used to determine any significant changes between the fractions tested.*p-value < 0.05, **p-value < 0.01, ***p-value < 0.001.

involved in antigen processing and MHC presentation that were dysregulated (Fig. 2A; Fig. 3A). In contrast to the previous study, which measured mRNA levels, we observed mildly decreased protein expression levels compared to mock-infected cells. This apparent discrepancy in the antiviral responses may be an artefact of using an in vitro cell culture system versus a fully immunocompetent animal model, or a result of

Fig. 4. Gene ontology analyses of up-regulated and down-regulated proteins. The proteins identified in Table 1 were imported into the DAVID gene ontology suite of programs at the NIAID, gene identifications converted by that program, and ontological functions determined by GOTERM. Only ontological functions whose *p* values are <0.05 are indicated. □, 5 hpi; ■, 24 hpi.

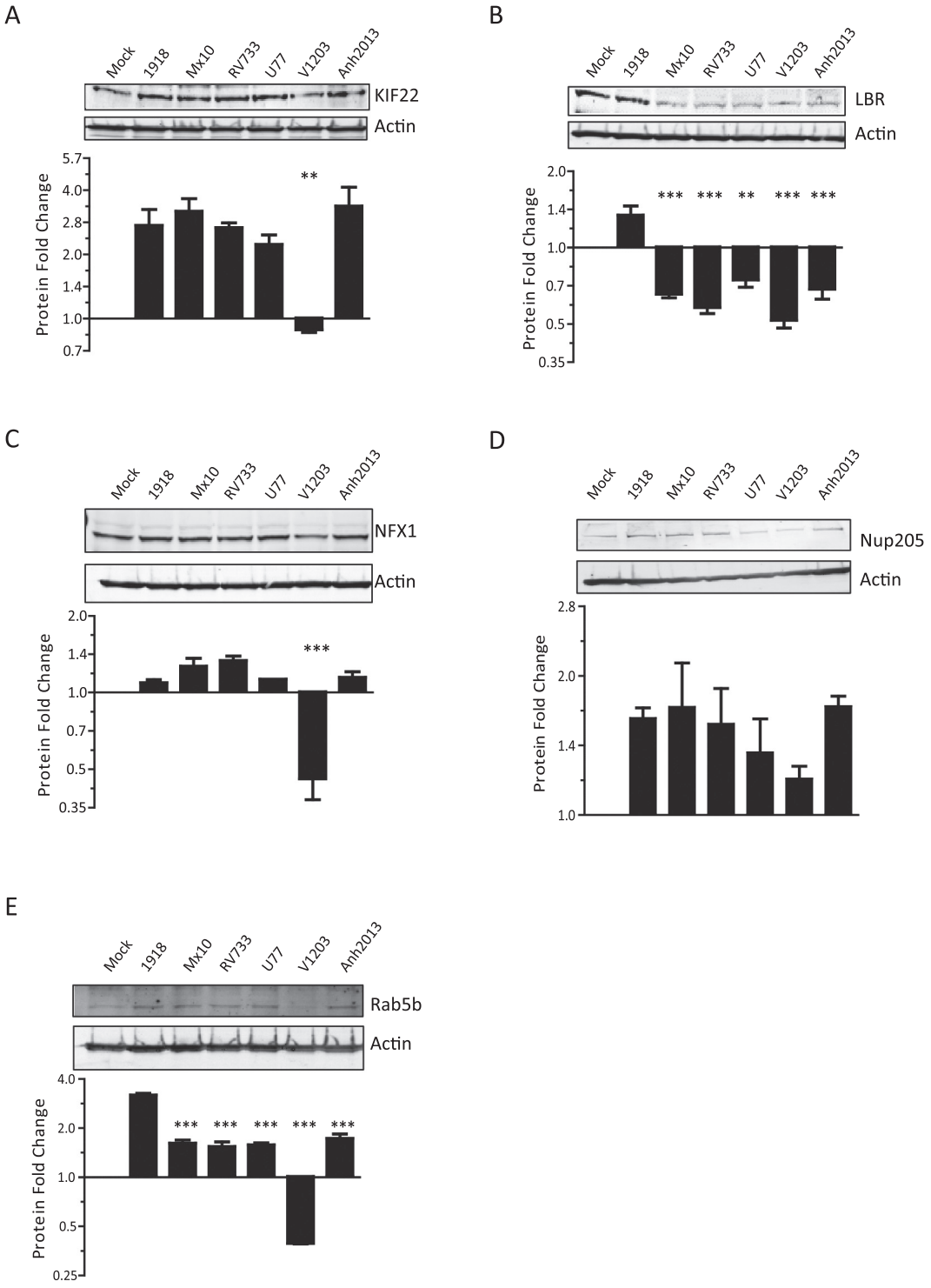

Fig. 6. Host protein expression profiles after IAV infection.A549 cells were infected with various influenza A viruses at an MOI of 7. Cell lysates were collected at 24 hpi and analyzed by Immunoblot. Protein expression was quantified by densitometry and normalized to the expression of actin. The fold increase in protein expression was determined by comparing mock and infected samples. The mean and standard error of the mean was calculated from three separate protein expression experiments. A one-way Anova with a Dunnett post-test was used to determine any significant changes between the strains tested and 1918.*p-value < 0.05, **p-value < 0.01, ***p-value < 0.001.

variation between two different technologies. Thus, we investigated a more highly affected pathway.

Our proteomic analysis pointed to the dysregulation of the AKT/mTOR pathway by the 1918 virus. Using a variety of cell-based assays we verified the altered expression states of proteins involved in this pathway and the altered phosphorylation state of the AKT/mTOR pathway with 1918 infection. Furthermore, we then demonstrated that among our panel of different viruses, only the 1918 strain was sensitive to the effects of rapamycin, suggesting that 1918 has a unique way of utilizing the AKT/mTOR pathway to promote viral replication by maintaining mTORC1 activation. This distinct response to the modulation of the AKT/mTOR pathway could be a factor which plays a role in conferring the unique and significant virulence and/or transmissibility of this strain.

The PI3K/AKT/mTOR pathway is known to play a role in viral replication of a number of RNA and DNA viruses by regulating apoptosis, cell

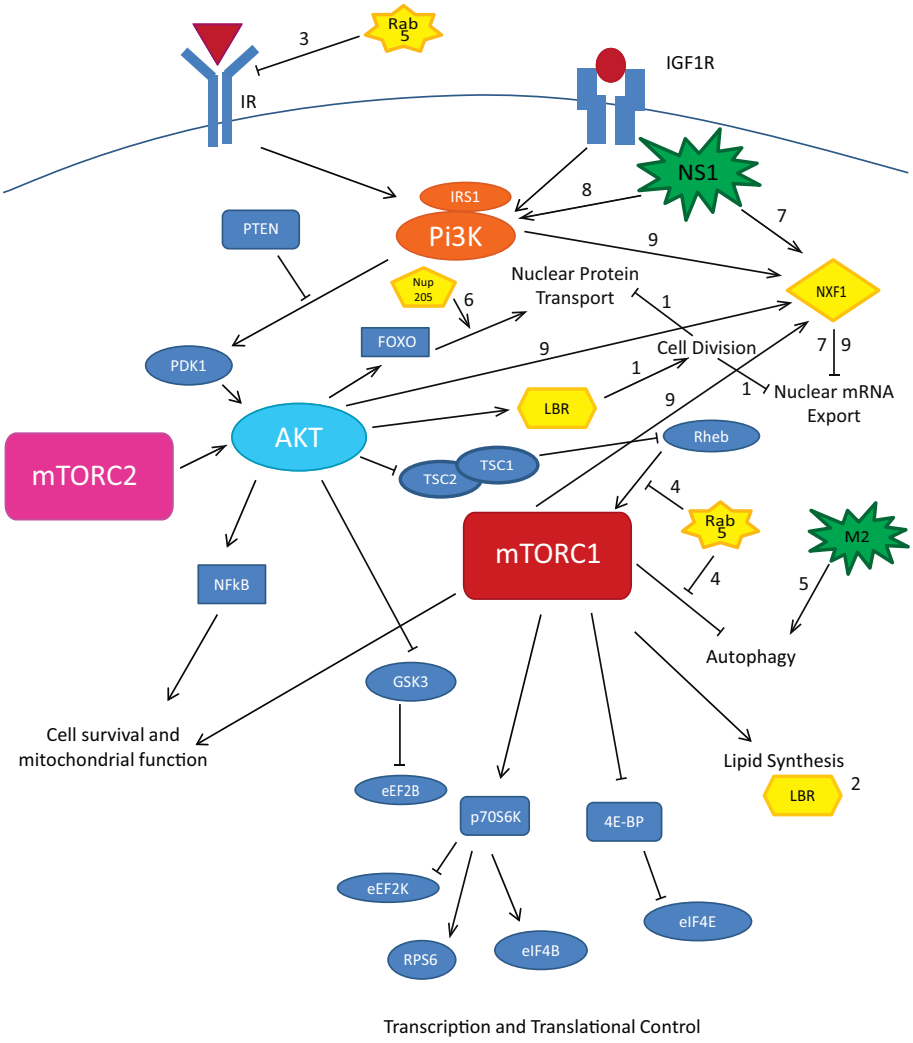

Fig. 7. Proposed model for the interaction of LBR, Rab5, Nup205, and NXF1 in the PI3K/mTOR/AKT signaling pathway. The PI3K/mTOR/AKT pathway plays a role in protein and lipid synthesis, metabolic processes and cell survival and proliferation. This pathway is also necessary to promote viral replication. Four cellular proteins have been shown to be differentially regulated during influenza virus infection. We propose that these proteins tie into the PI3K/mTOR/AKT pathway to facilitate viral replication. (1) LBR is a structural component of the nuclear envelope. Activation of LBR causes the destabilization of the nuclear envelope and induction of cell division, affecting active transport of material across the nuclear membrane. (2) LBR has sterol reductase activity, a component necessary for lipid synthesis, and lipogenesis is controlled by this pathway. Rab5 (3) interferes with insulin-mediated activation of PI3K and (4) inhibits mTORC1 activation by sequestering it away from the lysosomal compartment which subsequently affects downstream autophagy regulation. (5) The M2-ion channel of influenza virus has a role in subverting autophagy. (6) Nup205 is a component of the nuclear pore complex and acts as a regulatory gate controlling the size of proteins passing through the nuclear envelope. (7) The viral protein NS1 interacts with NXF1 and inhibits cellular mRNA export from the nucleus. (8) NS1 can also activate PI3K.(9) PI3K, mTOR and AKT activation has been shown to inhibit NFX1-mediated export of cellular mRNAs.

survival and host transcription and translation [8,13]. When PI3K is activated, it triggers AKT phosphorylation, which in turn leads to mTOR activation [5,20,22,31,72,73,77–79,84]. mTOR, a serine/threonine signaling kinase, forms two distinct complexes. The first, mTORC1 consists of mTOR, Raptor, Glb and DEPTOR and acts as a master growth regulator [44,45]. It controls major anabolic processes by activating protein synthesis, lipogenesis and energy metabolism, and inhibiting autophagy [33,38,44]. The second complex, mTORC2, comprised of mTOR, Rictor, GbL, Sin1, PRR5/Protor-1 and DEPTOR regulates cell proliferation [25,72]. mTORC2 functions as a regulatory kinase of AKT, PKCα and SGK1 [5,72,73,84].mTORC1 and AKT subsequently activate GSK3, p70S6K and 4E-BP and their effector proteins to initiate host transcription and translation.Many viruses are able to manipulate GSK3, p70S6K, 4E-BP, and their effectors, to inhibit cellular transcription and translation and allow for the production of viral proteins [9–11,14,19,63,76,93]. Our results demonstrate a suppression of the PI3K/AKT/mTOR pathway, which includes many of the proteins responsible for cellular transcription and translation (Fig. 8). It is likely that influenza viruses use inhibition of this pathway to minimize cellular transcription and translation while augmenting viral transcription and protein production.It is widely known that influenza virus infection shuts off host transcription and translation by decreasing production of cellular mRNA and the nucleocytoplasmic transport of cellular mRNA [27,41–43]. Previously, we demonstrated that viral translation increased in response to the suppression of the mTOR pathway during infection with PR8 but production of progeny virus was impaired [96]. This supports our finding, for the observed temporal depression of the mTOR pathway at early time points. This suppression of the the mTOR pathway is necessary to promote viral translation, a necessary requirement to promote viral genome replication and once ample viral proteins have been synthesized the pathway returns to a steady state level to allow for the continuation of the viral life cycle and production of viral progeny.

The eIF4F complex, made up of eIF4E, a downstream effector molecule of mTORC1 responsible for binding the cap of cellular mRNAs, the RNA helicase eIF4A, and eIF4G, a scaffolding protein, is necessary for protein translation. However, it was demonstrated that when eIF4E is functionally impaired, influenza translation still occurs [9]. The virus was able to overcome the need for eIF4E by the presence of the viral

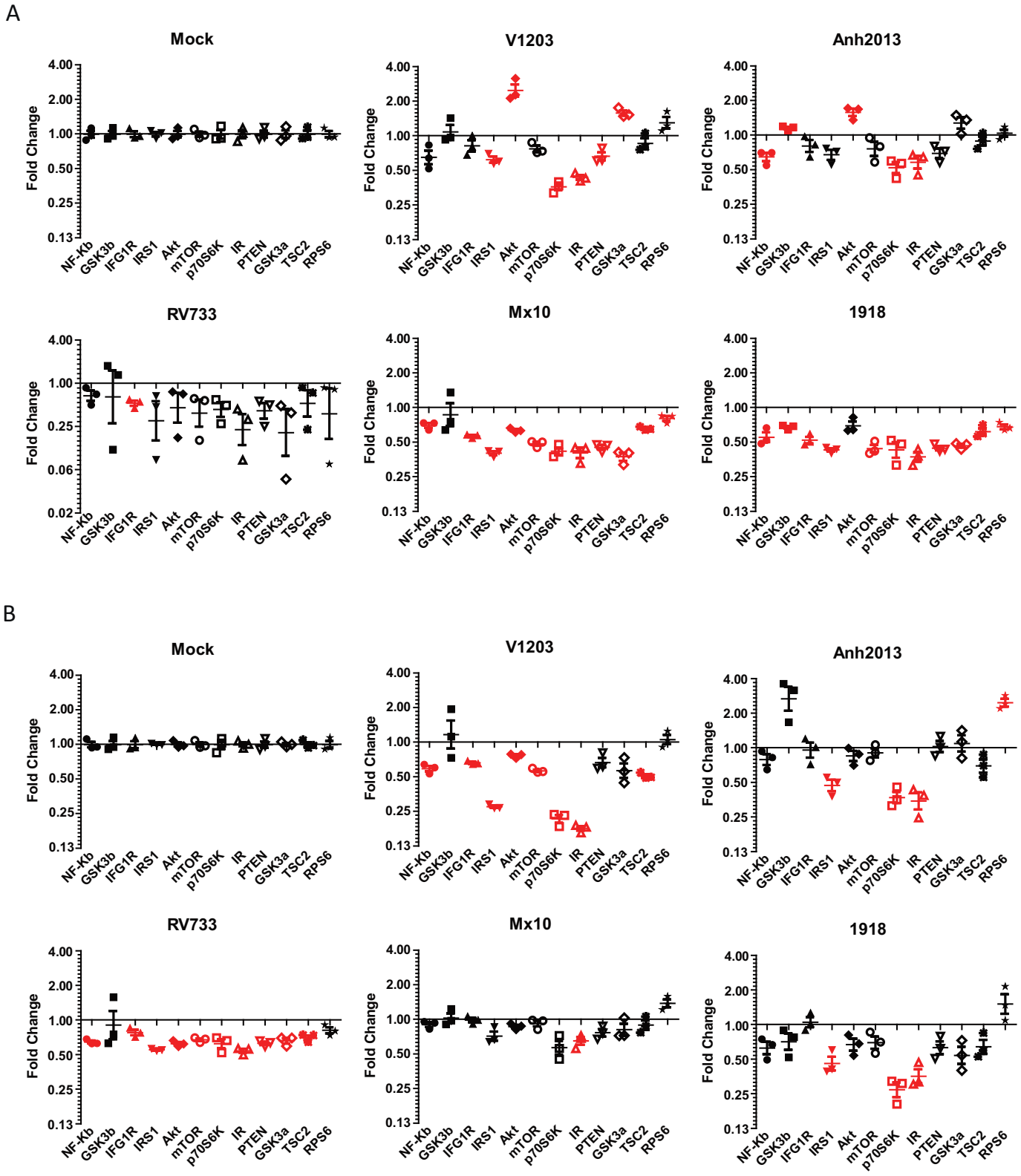

Fig. 8. The phosphorylation state of proteins found in the mTOR/AKT signaling cascade.A549 cells were infected with various influenza A viruses at an MOI of 7.Cells lysates were collected at (A) 5 hpi and (B) 24 hpi and their phosphorylation states were assessed using a luminex-bead based phosphoprotein assay. Each of three biologic replicates was analyzed in triplicate and the means and standard errors are presented. *t*-tests were used to determine any significant changes in the phosphorylation state of these proteins. Data points presented in red are significantly altered compared to the cognate mock samples with p values < 0.05.

polymerase. The viral polymerase remains associated with the cap of the viral mRNA and eIF4A and eIF4G are subsequently recruited to maintain a functional eIF4F complex to initiate viral translation [9]. The inhibition of eIF4E activation is the likely mechanism causing the suppression of host translational activities by preventing the formation of a functional eIF4F complex. Viral translation can still occur, since the

viral polymerase is capable of functioning as eIF4E to allow for the formation of the eIF4F complex. Our results demonstrate the inhibition of mTOR, which prevents eIF4E activation, and supports the observation that influenza virus infection inhibits cellular transcription and translation (Fig. 7). Interestingly, we observed that the inhibition of mTORC1 with rapamycin for prolonged periods does not impair virus replication for most of the viruses we tested, whereas our previous study demonstrated that PR8 replication was impaired with prolonged rapamycin treatment [96]. We observed a similar situation for the 1918 virus. PR8, isolated in 1934 and descended from the 1918 virus, is one of the oldest isolates that is routinely studied. The other strains tested in this study were isolated more recently, from 2007 to 2013. We could be observing an evolutionary adaptation in how the viruses use the PI3K/AKT/mTOR pathway that could be responsible for these differences.

Nucleocytoplasmic transport of molecules across the nuclear membrane is also important for influenza virus replication. NXF1 is essential for the transport of cellular mRNAs, containing exon-exon junctions, out of the nucleus [15,68]. NXF1 is also essential for influenza virus replication [6,32,40,74] but the role of this pathway has not been well defined. While the export of viral RNP structures out of the nucleus occurs through the interaction between NEP and the CREM1 export pathway [58], the NS1 protein is able to interact with NXF1 and prevent the export of cellular mRNAs [74] (Fig. 7). We observed that influenza infection caused NXF1 to be upregulated at later time points, which could be the host's attempt to subvert the effects of NS1. Alternatively, the virus may also be able to use the NXF1 export pathway in addition to the CREM1 pathway. Interestingly, the influenza NS1 protein is also capable of binding p85β, the PI3K regulatory subunit, and stimulating PI3K kinase activity [20,22,31,77–79] (Fig. 7). However, the activation of PI3K activity is limited to IAV while PI3K activation remains unchanged by influenza B viruses [21]. One study linked the PI3K/AKT/mTOR pathway as a regulator of NXF1-mediated cellular mRNA export from the nucleus [67]. Inhibition of PI3K, AKT and mTOR activation allowed for increased NXF1 mediated-export of cellular mRNA from the nucleus and activation of the pathway caused retention of cellular mRNA in the nucleus[67] (Fig. 7). We tested three H1N1 strains, 1918, Mx10 and RV733, and two avian-origin influenza strains, V1203 (H5N1) and Anh2013 (H7N9) that exhibit high virulence in human infections. Interestingly, all three H1N1 strains demonstrated a decrease in mTOR and AKT activation; 1918- and Mx10-mediated mTOR and AKT activation occurred at early time points post infection, while the decrease occurred at later time points for RV733, suggesting reduced upstream activation of PI3K, which was confirmed by the observed inhibition of IR and IGF1R activation. Of note, the two avian influenza viruses caused significant AKT activation, suggesting instead the activation of PI3K for these viruses. Interestingly, IR activation was depressed during infection with the avian strains; however, IGF1R remained at baseline levels suggesting some degree of PI3K activation. Thus, influenza virus-induced signaling appears to be strain specific. Our data demonstrated an initial downregulation of NXF1 in the nuclear fraction and an upregulation in the cytoplasmic fraction at 5 h post infection during 1918 influenza virus infection (Fig. 5), suggesting a shift away from normal steady state equilibrium towards nuclear export of mRNA. By 24 hpi, NXF1 expression returned to steady state levels in the nuclear fraction but remained slightly upregulated in the cytoplasmic fraction (Fig.5). This correlated with the observed inhibition of the AKT/mTOR pathway at 5 hpi and then its return to steady state levels at 24 hpi. Interestingly, when the expression profiles of NXF1 were compared to other viruses at 24 hpi, most viruses responded similarly to the 1918 strain (Fig. 6). The inhibition of the AKT/mTOR pathway and increased shift of NXF1 into the cytoplasm at early time points is consistent with increased NXF1-mediated mRNA nuclear export and may indicate a novel role for this pathway in viral replication. Since expression of NS1 is linked to the retention of cellular mRNA in the nucleus [74,81], this may favor the export of viral mRNA. Furthermore, retention of host mRNA in the nucleus could aid in virus-mediated cap snatching, a unique phenomenon in which the first 10–20 nucleotides of cellular pre-mRNA is removed and used as primer for viral mRNA synthesis. Furthermore, the accumulation of cellular mRNA in the nucleus would subsequently decrease host translation allowing the host machinery to be available for viral replication. Our data show that the inhibition of mTORC1 does not affect viral replication for most viruses, confirming the idea that the host will favor virus replication over cellular transcription/translation. This suggests that the viral-induced inhibition of the PI3K/AKT/mTOR pathway and its downstream effect on NXF1 could play a role in diverting host machinery towards supporting viral functionality. Interestingly, the inhibition of mTORC1 has a unique effect on 1918 replication. We observed inhibition of 1918 replication by the prolonged inhibition of mTORC1, suggesting that a balance between mTOR inhibition for some steps in the viral life cycle and its ability to maintain production of progeny virus must be maintained, a unique finding for this strain of influenza.

LBR and Rab5 were two proteins differentially expressed in 1918-infected cells compared to other strains of influenza virus. LBR, a dual functioning protein, contains an N-terminal domain found in the nucleoplasm where it interacts with B-lamins, heterochromatin and chromatin binding proteins, aiding in the maintenance of chromatin structure as well as nucleus reformation after mitosis, and a C-terminal domain anchoring LBR to the inner nuclear membrane [18,52,54,66,82,94,95]. The LBR C-terminal domain has sterol reductase activity [64,71,80], which is important for cholesterol synthesis. The role that LBR plays in maintaining the lamina structure of the nuclear membrane may indirectly regulate transport of viral gene products in and out of the nucleus (Fig. 7). Little is known about the interaction between LBR and the PI3K/AKT/mTOR pathway; however, it was recently discovered that AKT is able to phosphorylate Arginine-Serine residues in the N-terminal region of LBR [90]. The phosphorylation of this protein causes a conformational change, detaching the peripheral heterochromatin from the inner nuclear membrane, causing LBR to become highly mobile, thus fostering the destabilization of the nuclear envelope for mitosis [90]. During this process, the stability of the nuclear pores complexes will be compromised, impairing nuclear transport. The inducible sterol reductase activity of LBR could also have a role in the production of lipids required for viral replication (Fig. 7). A previous study identified LBR as being moderately upregulated when A549 cells were infected with a 2009 pandemic H1N1 isolate by mass spectrometry [16]. Unfortunately, we were not able to demonstrate similar results in our study; however, the isolate (Mx10) used in this study was not employed in mass spectrometry experiments, but was used solely for biological validation, an approach which was not done in the previous study. Therefore, a direct comparison of results is difficult. We show that LBR was upregulated at both 5 h and 24 h after infection with 1918, an observation that was distinctively different from the other strains tested in our study. Our findings suggest a novel role of LBR in the 1918 virus life cycle by accommodating increased nuclear stability, promoting viral nuclear transport, and aiding lipid production involved in virus budding and egress; however, further studies to confirm the role of LBR in the 1918 life cycle are needed.

Rab5 is a GTPase which regulates the endocytic pathway [97], controls homotypic fusion of endosomes [3,30], vesicle movement on microtubules [35] and Rab GTPase conversion [70]. The elevated expression of Rab5 GTPases has been implicated in decreasing insulin-mediated activation of PI3K [51] downstream of mTORC1 activation [7,24,50] (Fig. 7). The decline in mTORC1 activity in circumstances of elevated Rab5 is the result of Rab5 misdirecting mTORC1 away from lysosomal compartments and into swollen vacuolar-like structures, preventing mTORC1 from being phosphorylated by Rheb or Rag [7,50]. We showed Rab5b is upregulated during infection with 1918 influenza virus but not by the other strains assessed (Table 1, Figs. 5 and 6), indicating Rab5 expression may have a unique role in the 1918 virus life cycle. These results are consistent with previous reports that Rab5 expression inhibits the PI3K/AKT/mTOR signaling cascade [7,24,50].

Based on these reports, we may extend the possibility that 1918 infection induces an increase in Rab5 expression as a mechanism to inhibit mTORC1 phosphorylation through its ability to sequester mTORC1 away from sites of PI3K/AKT/mTOR signaling activity [7,24,50]. However, our results also demonstrate a temporal depression of the PI3K/AKT/mTOR pathway by the other strains assessed (Fig. 8). While Rab5 may play a role in the depression of this pathway for 1918, it is not the only factor responsible, since 1918 replication was distinctly sensitivity to the inhibition of mTORC1 phosphorylation by rapamycin treatment (Fig. 9). The distinct expression profile of Rab5 and its sensitivity to mTORC1 inhibition by 1918 infection compared to other influenza strains may be correlated; however, follow up investigations into the role of Rab5 would be needed to fully understand this mechanism of action. mTORC1 is known to negatively regulate autophagy; therefore, a decrease in mTORC1 activity by Rab5 expression will have a positive effect on the induction of autophagy activity [50]. Autophagy is responsible for the degradation of cellular organelles and protein aggregates of long-lived proteins [55]. Macroautophagy is the best understood pathway of autophagy and has roles in both innate and adaptive immune responses [75]. A two-membrane vesicle forms around its target to generate an autophagic vesicle. This vesicle will then fuse with late endosomes and lysosomes for substrate degradation. Many viruses have evolved subversion strategies, which allow them to benefit from host-mediated autophagy [4,23,26,34,46,69,85]. The influenza virus

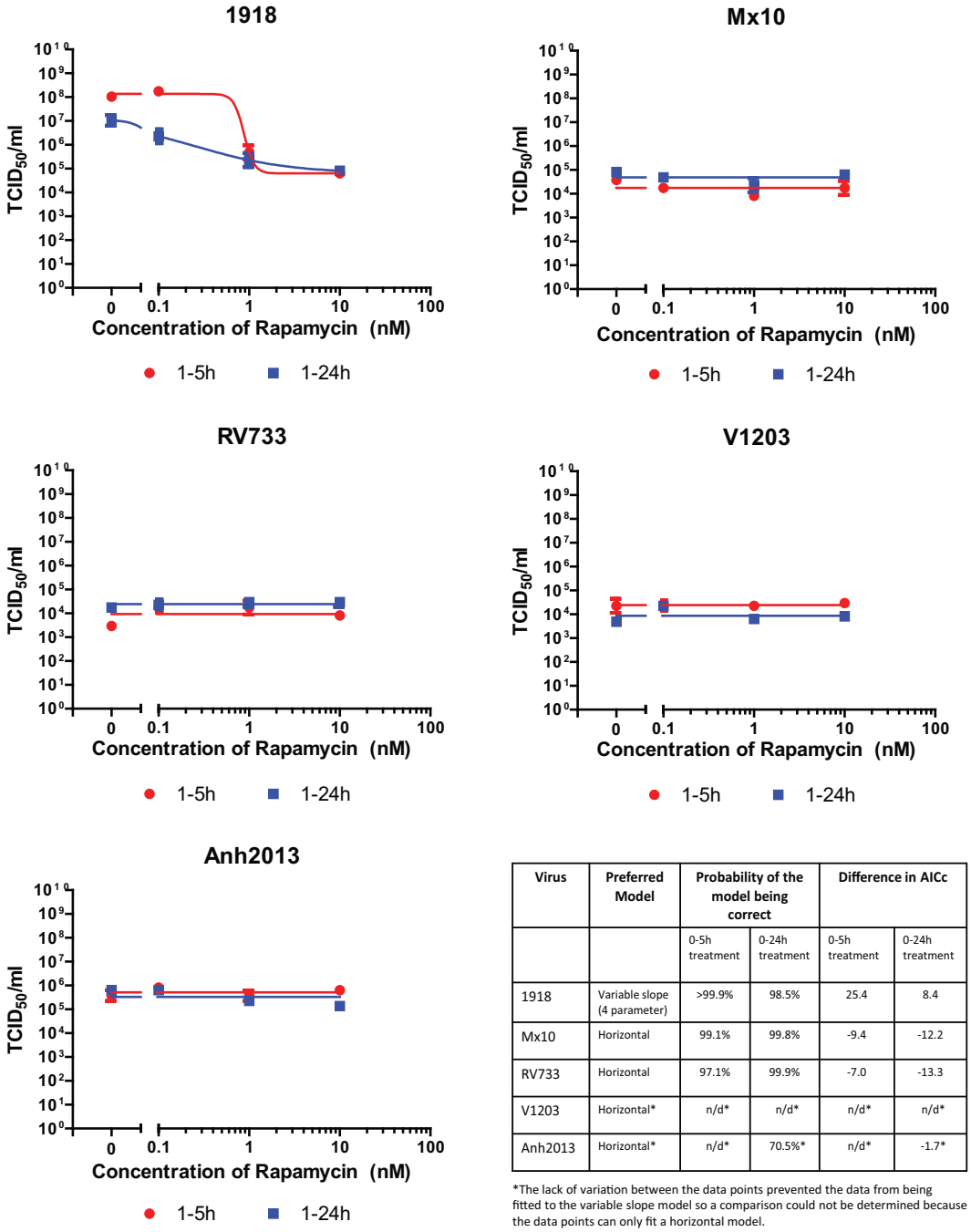

Virus	Preferred Model	Probability of the model being correct		Difference in AICc	
		0-5h treatment	0-24h treatment	0-5h treatment	0-24h treatment
1918	Variable slope (4 parameter)	>99.9%	98.5%	25.4	8.4
Mx10	Horizontal	99.1%	99.8%	-9.4	-12.2
RV733	Horizontal	97.1%	99.9%	-7.0	-13.3
V1203	Horizontal*	n/d*	n/d*	n/d*	n/d*
Anh2013	Horizontal*	n/d*	70.5%*	n/d*	-1.7*

*The lack of variation between the data points prevented the data from being fitted to the variable slope model so a comparison could not be determined because the data points can only fit a horizontal model.

Fig. 9. Increased suppression of mTORC1 activation negatively affects 1918 viral replication. A549 cells were infected with various influenza A viruses at an MOI of 0.01. Cells were treated with varying amounts of rapamycin for 5 or 24 h.At 48 hpi, supernatants were harvested and virus was titrated. A model comparsion was performed using horizontal line and 4-parameter variable slope models to fit the data. A horizontal line model suggests there was no effect on virus replication by rapamycin treatment, while a 4-parameter variable slope model predicts that there was a dose-dependent response to treatment.

M2-ion channel protein plays a role in subverting autophagy by blocking fusion of the autophagosome with the lysosome [4,26] and can further utilize the autophagy machinery as a source of materials needed for virus budding and virion stability [4] (Fig. 7). While the 1918 virus may use Rab5 as an inhibitor of the PI3K/AKT/mTOR pathway, subsequently causing the activation of autophagy, other strains may have evolved alternative strategies to do the same thing.

In conclusion, we found that 1918 infection temporally inhibits the mTOR pathway, while effectively promoting viral replication; however, the robust and prolonged depression of mTOR by rapamycin severely impairs 1918 replication. This suggests that 1918 virus-mediated mTOR activity inhibition is tightly regulated both temporally and by degree to promote 1918 replication. Deviation from this balance of activity would have detrimental effects. Our study suggests that infection of A549 human lung cells with influenza viruses alters host nucleocytoplasmic shuttling of molecules across the nuclear membrane, cellular transcription and translation activities, and host synthesis of lipids through a dysregulation of the PI3K/AKT/mTOR pathway. Among the viruses we compared, we observed a unique expression profile of two host proteins, LBR and Rab5b proteins in 1918 infected cells. The temporal increase in Rab5b expression could play key roles in transient depression of the PI3K/AKT/mTOR pathway. Likewise, the general upregulation of LBR could have a role in increased cholesterol synthesis and its overall increase in post-translational phosphorylation by AKT due to increased expression levels, which could have downstream effects on the stability of the nuclear envelope and subsequently nuclear transport. The findings we have presented in this study complement and bridge some gaps between other reports, together providing a more coherent picture of how influenza viruses highjack the host response and the possible mechanisms required to mediate virus replication. Moreover, our work paves the way for further research on the relationship between 1918 infection and the PI3K/AKT/mTOR signaling pathway and the host mechanisms responsible for facilitating virus replication and in determining levels and severity of pathogenesis.

Supplementary data to this article can be found online at https://doi.org/10.1016/j.ebiom.2018.05.027.

Acknowledgements

The authors thank Kolawole Opanubi for expert technical assistance, Dr. Ming Yang for anti-influenza virus NP monoclonal hybridoma cells, and Dr. Yoshihiro Kawaoka for the influenza virus reverse genetics system.

Funding Sources

This research was supported by grants # PAN-83159 and MOP-106713 from the Canadian Institutes of Health Research (CIHR) to KMC, and by general facility funding from the Public Health Agency of Canada to CR and DK.

Conflicts of Interest

The authors declare no conflicts of interest.

Author Contributions

CR, DK and KMC designed the study.

KMC prepared the SILAC-labeled cells.

DK infected and processed the SILAC-labeled cells for mass spectrometry.

CR performed other experimental work related to, and prepared, Figs. 1, 5–9.

KMC performed statistical and pathway analyses and prepared Figs. 2–4; S1, S2; and Tables 1, 2.KMC performed statistical and pathway analyses and prepared Figs. 2–4; S1, S2; and Tables 1, 2.

All authors wrote and edited the text, and approved the final version. genesis.

References

[1] Ahmed R, Oldstone MBA, Palse P. Protective immunity and susceptibility to infectious diseases: lessons from the 1918 influenza pandemic. Nat Immunol 2007;8:1188–93.
[2] Baas T, Baskin CR, Diamond DL, Garcia-Sastre A, Bielefeldt-Ohmann H, Tumpey TM, et al. Integrated molecular signature of disease: analysis of influenza virus-infected macaques through functional genomics and proteomics. J Virol 2006;80:10813–28.
[3] Barbieri MA, Li GP, Colombo MI, Stahl PD. Rab5, an early acting endosomal Gtpase, supports in-vitro endosome fusion without Gtp hydrolysis. J Biol Chem 1994;269:18720–2.
[4] Beale R, Wise H, Stuart A, Ravenhill BJ, Digard P, Randow F. A LC3-interacting motif in the influenza avirus M2 protein is required to subvert autophagy and maintain Virion stability. Cell Host Microbe 2014;15:239–47.
[5] Betz C, Stracka D, Prescianotto-Baschong C, Frieden M, Demaurex N, Hall MN. mTOR complex 2-Akt signaling at mitochondria-associated endoplasmic reticulum membranes (MAM) regulates mitochondrial physiology. Proc Nat Acad Sci USA 2013;110:12526–34.
[6] Brass AL, Huang IC, Benita Y, John SP, Krishnan MN, Feeley EM, et al. The IFITM proteins mediate cellular resistance to influenza A H1N1 virus, West Nile virus, and dengue virus. Cell 2009;139:1243–54.
[7] Bridges D, Fisher K, Zolov SN, Xiong TT, Inoki K, Weisman LS, et al. Rab5 proteins regulate activation and localization of target of rapamycin complex 1. J Biol Chem 2012;287:20913–21.
[8] Buchkovich NJ, Yu Y, Zampieri CA, Alwine JC. The TORrid affairs of viruses: effects of mammalian DNA viruses on the PI3K-Akt-mTOR signalling pathway. Nat Rev Microbiol 2008;6:265–75.
[9] Buegui I, Yanguez E, Sonenberg N, Nieto A. Influenza virus mRNA translation revisited: is the eIF4E cap-binding factor required for viral mRNA translation? J Virol 2007;81:12427–38.
[10] Bushell M, Sarnow P. Hijacking the translation apparatus by RNA viruses. J Cell Biol 2002;158:395–9.
[11] Connor JH, Lyles DS. Vesicular stomatitis virus infection alters the eIF4F translation initiation complex and causes dephosphorylation of the eIF4E binding protein 4E-BP1. J Virol 2002;76:10177–87.
[12] Coombs KM, Berard A, Xu W, Krokhin O, Meng X, Cortens JP, et al. Quantitative proteomic analyses of influenza virus-infected cultured human lung cells. J Virol 2010;84:10888–906.
[13] Cooray S. The pivotal role of phosphatidylinositol 3-kinase-Akt signal transduction in virus survival. J Gen Virol 2004;85:1065–76.
[14] Cuesta R, Xi QR, Schneider RJ. Adenovirus-specific translation by displacement of kinase Mnk1 from cap-initiation complex eIF4F. EMBO J 2000;19:3465–74.
[15] Cullen BR. Nuclear mRNA export: insights from virology. Trends Biochem Sci 2003;28:419–24.
[16] Dapat C, Saito R, Suzuki H, Horigome T. Quantitative phosphoproteomic analysis of host responses in human lung epithelial (A549) cells during influenza virus infection. Virus Res 2014;179:53–63.
[17] Dennis G, Sherman BT, Hosack DA, Yang J, Gao W, Lane HC, et al. DAVID: database for annotation, visualization, and integrated discovery. Genome Biol 2003;4:P3.
[18] Duband-Goulet I, Courvalin JC, Buendia B. LBR, a chromatin and lamin binding protein from the inner nuclear membrane, is proteolyzed at late stages of apoptosis. J Cell Sci 1998;111:1441–51.
[19] Edgil D, Polacek C, Harris E. Dengue virus utilizes a novel strategy for translation initiation when cap-dependent translation is inhibited. J Virol 2006;80:2976–86.
[20] Ehrhardt C, Marjuki H, Wolff T, Nurnerg B, Planz O, Pleschka S, et al. Bivalent role of the phosphatidylinositol-3-kinase (PI3K) during influenza virus infection and host cell defence. Cell Microbiol 2006;8:1336–48.
[21] Ehrhardt C, Wolff T, Ludwig S. Activation of phosphatidylinositol 3-kinase signaling by the nonstructural NS1 protein is not conserved among type a and B influenza viruses. J Virol 2007;81:12097–100.
[22] Ehrhaedt C, Wolff T, Pleschka S, Planz O, Beermann W, Bode JG, et al. Influenza A virus NS1 protein activates the PI3K/Akt pathway to mediate antiapoptotic signaling responses. J Virol 2007;81:3058–67.
[23] Feng ZD, Hensley L, McKnight KL, Hu FY, Madden V, Ping LF, et al. A pathogenic picornavirus acquires an envelope by hijacking cellular membranes. Nature 2013;496:367.
[24] Flinn RJ, Yan Y, Goswami S, Parker PJ, Backer JM. The late endosome is essential for mTORC1 signaling. Mol Biol Cell 2010;21:833–41.
[25] Frias MA, Thoreen CC, Jaffe JD, Schroder W, Sculley T, Carr SA, et al. mSin1 is necessary for Akt/PKB phosphorylation, and its isoforms define three distinct mTORC2s. Curr Biol 2006;16:1865–70.
[26] Gannage M, Dormann D, Albrecht R, Dengjel J, Torossi T, Ramer PC, et al. Matrix protein 2 of influenza A virus blocks autophagosome fusion with lysosomes. Cell Host Microbe 2009;6:367–80.
[27] Garfinkel MS, Katze MG. Translational control by influenza-virus - selective translation is mediated by sequences within the viral messenger-Rna 5′-untranslated region. J Biol Chem 1993;268:22223–6.
[28] Geiss GK, Salvatre M, Tumpey TM, Carter VS, Wang XY, Basler CF, et al. Cellular transcriptional profiling in influenza A virus-infected lung epithelial cells: the role of the nonstructural NS1 protein in the evasion of the host innate defense and its potential contribution to pandemic influenza. Proc Natl Acad Sci U S A 2002;99:10736–41.

[29] Gilar M, Olivova P, Daly AE, Gebler JC. Orthogonality of separation in two-dimensional liquid chromatography. Anal Chem 2005;77:6426–34.
[30] Gorvel JP, Chavrier P, Zerial M, Gruenberg J. Rab5 controls early endosome fusion Invitro. Cell 1991;64:915–25.
[31] Hale BG, Jackson D, Chen YH, Lamb RA, Randall RE. Influenza A virus NS1 protein binds p85 beta and activates phosphatidylinositol-3-kinase signaling. Proc Natl Acad Sci USA 2006;103:14194–9.
[32] Hao LH, Sakurai A, Watanabe T, Sorensen E, Nidom CA, Newton MA, et al. Drosophila RNAi screen identifies host genes important for influenza virus replication. Nature 2008;454 890-U46.
[33] Hay N, Sonenberg N. Upstream and downstream of mTOR. Genes Dev 2004;18: 1926–45.
[34] Heaton NS, Randall G. Dengue virus-induced autophagy regulates lipid metabolism. Cell Host Microbe 2010;8:422–32.
[35] Hoepfner S, Severin F, Cabezas A, Habermann B, Runge A, Giilooly D, et al. Modulation of receptor recycling and degradation by the endosomal kinesin KIF16B. Cell 2005;121:437–50.
[36] Huang DW, Sherman BT, Lempicki RA. Systematic and integrative analysis of large gene lists using DAVID bioinformatics resources. Nat Protoc 2009;4:44–57.
[37] Huang QL, Wang L, Bai SY, Lin WS, Chen WN, Lin JY, et al. Global proteome analysis of hepatitis B virus expressing human hepatoblastoma cell line HepG2. J Med Virol 2009;81:1539–50.
[38] Jacinto E, Lorberg A. TOR regulation of AGC kinases in yeast and mammals. Biochem J 2008;410:19–37.
[39] Jagger BW, Wise HM, Kash JC, Walters KA, Wills NM, Xiao YL, et al. An overlapping protein-coding region in influenza A virus segment 3 modulates the host response. Science 2012;337:199–204.
[40] Karlas A, Machuy N, Shin Y, Pleissner KP, Artarini A, Heuer D, et al. Genome-wide RNAi screen identifies human host factors crucial for influenza virus replication. Nature 2010;463:818–22.
[41] Katze MG, Chen YT, Krug RM. Nuclear cytoplasmic transport and Vai Rna-independent translation of influenza viral messenger-Rnas in late adenovirus-infected cells. Cell 1984;37:483–90.
[42] Katze MG, Decorato D, Krug RM. Cellular messenger-Rna translation is blocked at both initiation and elongation after infection by influenza-virus or adenovirus. J Virol 1986;60:1027–39.
[43] Katze MG, Krug RM. Metabolism and expression of Rna polymerase-Ii transcripts in influenza virus-infected cells. Mol Cell Biol 1984;4:2198–206.
[44] Kim DH, Sarbassov DD, Ali SM, King JE, Latek RR, Eedjument-Bromage H, et al. MTOR interacts with raptor to form a nutrient-sensitive complex that signals to the cell growth machinery. Cell 2002;110:163–75.
[45] Kim DH, Sarbassov DD, Ali SM, Latek RR, Guntur KVP, Eedjument-Bromage H, et al. G beta L, a positive regulator of the rapamycin-sensitive pathway required for the nutrient-sensitive interaction between raptor and mTOR. Mol Cell 2003;11: 895–904.
[46] Klein KA, Jackson WT. Picornavirus subversion of the autophagy pathway. Viruses-Basel 2011;3:1549–61.
[47] Kobasa D, Jones SM, Shinya K, Kash JC, Copps J, Ebihara H, et al. Aberrant innate immune response in lethal infection of macaques with the 1918 influenza virus. Nature 2007;445:319–23.
[48] Kroeker AL, Ezzati P, Halayko AJ, Coombs KM. Response of primary human airway epithelial cells to influenza infection – a quantitative proteomic study. J Proteome Res 2012;11:4132–6.
[49] La Gruta NL, Kedzierska K, Stambas J, Doherty PC. A question of self-preservation: immunopathology in influenza virus infection. Immunol Cell Biol 2007;85:85–92.
[50] Li L, Kim E, Yuan HX, Inoki K, Goraksha-Hicks P, Schiesher RL, et al. Regulation of mTORC1 by the Rab and Arf GTPases. J Biol Chem 2010;285:19705–9.
[51] Lodhi IJ, Bridges D, Chiang SH, Zhang YL, Cheng A, Geletka LM, et al. Insulin stimulates phosphatidylinositol 3-phosphate production via the activation of Rab5. Mol Biol Cell 2008;19:2718–28.
[52] Makatsori D, Kourmouli N, Polioudaki H, Shultz LD, Mclean K, Theodoropoulos PA, et al. The inner nuclear membrane protein lamin B receptor forms distinct microdomains and links epigenetically marked chromatin to the nuclear envelope. J Biol Chem 2004;279:25567–73.
[53] Mcauley JL, Kedzierska K, Brown LE, Shanks GD. Host immunological factors enhancing mortality of young adults during the 1918 influenza pandemic. Front Immunol 2015;6.
[54] Meier J, Georgatos SD. Type-B Lamins remain associated with the integral nuclear-envelope protein P58 during mitosis - implications for nuclear reassembly. EMBO J 1994;13:1888–98.
[55] Mizushima N, Klionsky DJ. Protein turnover via autophagy: implications for metabolism. Annu Rev Nutr 2007;27:19–40.
[56] Morsens DM, Taubenberger JK. 1918 influenza, a puzzle with missing pieces. Emerg Infect Dis 2012;18:332–5.
[57] Nesvizhskii AI, Aebersold R. Interpretation of shotgun proteomic data - the protein inference problem. *Mol* Cell Proteomics 2005;4:1419–40.
[58] Neumann G, Hughes MT, Kawaoka Y. Influenza A virus NS2 protein mediates vRNP nuclear export through NES-independent interaction with hCRM1. EMBO J 2000;19: 6751–8.
[59] Neumann G, Kawaoka Y. Genetic engineering of influenza and other negative-strand RNA viruses containing segmented genomes. Adv Virus Res 1999;53(53): 265–300.
[60] Olstone MBA, Rosen H. Cytokine storm plays a direct role in the morbidity and mortality from influenza virus infection and is chemically treatable with a single sphingosine-1-phosphate agonist molecule. Curr Topics Microbiol Immunol 2014; 378:129–47.
[61] Oldstone MBA, Teijaro JR, Walsh KB, Rosen H. Dissecting influenza virus pathogenesis uncovers a novel chemical approach to combat the infection. Virology 2013;435: 92–101.
[62] Palese P, Shaw ML. Orthomyxoviridae: the viruses and their replication. In: Knipe DM, Howley PM, editors. Fields Virology. 5th ed. Philadelphia: Lippincott Williams & Wilkins; 2007.
[63] Piron M, Vende P, Cohen J, Poncet D. Rotavirus RNA-binding protein NSP3 interacts with eIF4GI and evicts the poly(A) binding protein from eIF4F. EMBO J 1998;17: 5811–21.
[64] Prakash A, Sengupta S, Aparna K, Kasbekar DP. The erg-3 (sterol Delta(14,15)-reductase) gene of Neurospora crassa: generation of null mutants by repeat-induced point mutation and complementation by proteins chimeric for human lamin B receptor sequences. Microbiology 1999;145:1443–51.
[65] Prevention. Types of Influenza Viruses. [Online]. Available http://www.cdc.gov/flu/about/viruses/types.htm; 2016, Accessed date: 17 June 2016.
[66] Pyrpasopoulou A, Meier J, Maison C, Simos G, Georgatos SD. The lamin B receptor (LBR) provides essential chromatin docking sites at the nuclear envelope. EMBO J 1996;15:7108–19.
[67] Quaresma AJC, Sievert R, Nickerson JA. Regulation of mRNA export by the PI3 kinase/AKT signal transduction pathway. Mol Biol Cell 2013;24:1208–21.
[68] Reed R, Cheng H. TREX, SR proteins and export of mRNA. Curr Opin Cell Biol 2005; 17:269–73.
[69] Reggiori F, Monastyrska I, Verheije MH, Cali T, Ulasli M, Bianchi S, et al. Coronaviruses hijack the LC3-I-positive EDEMosomes, ER-derived vesicles exporting short-lived ERAD regulators, for replication. Cell Host Microbe 2010;7:500–8.
[70] Rink J, Ghigo E, Kalaidzidis Y, Zerial M. Rab conversion as a mechanism of progression from early to late endosomes. Cell 2005;122:735–49.
[71] Roberti R, Bennati AM, Galli G, Caruso D, Maras B, Aisa C, et al. Cloning and expression of sterol Delta 14-reductase from bovine liver. Eur J Biochem 2002;269:283–90.
[72] Sarbassov DD, Ali SM, Kim DH, Guertin DA, Latek RR, Erdjument-Bromage H, et al. Rictor, a novel binding partner of mTOR, defines a rapamycin-insensitive and raptor-independent pathway that regulates the cytoskeleton. Curr Biol 2004;14:1296–302.
[73] Sarbassov DD, Guertin DA, Ali SM, Sabatini DM. Phosphorylation and regulation of Akt/PKB by the rictor-mTOR complex. Science 2005;307:1098–101.
[74] Satterly N, Tsai PL, Van Deursen J, Nussenzveig DR, Wang YM, Faria PA, et al. Influenza virus targets the mRNA export machinery and the nuclear pore complex. Proc Natl Acad Sci U S A 2007;104:1853–8.
[75] Schmid D, Munz C. Innate and adaptive immunity through autophagy. Immunity 2007;27:11–21.
[76] Schneider RJ, Mohr I. Translation initiation and viral tricks. Trends Biochem Sci 2003; 28:130–6.
[77] Shin YK, Li Y, Liu Q, Anderson DH, BAabiuk LA, Zhou Y. SH3 binding motif 1 in influenza a virus NS1 protein is essential for PI3K/Akt signaling pathway activation. J Virol 2007;81:12730–9.
[78] Shin YK, Liu Q, Tikoo SK, Babiuk LA, Zhou Y. Effect of the phosphatidylinositol 3-kinase/Akt pathway on influenza A virus propagation. J Gen Virol 2007;88:942–50.
[79] Shin YK, Liu Q, Tikoo SK, Babuik LA, Zhou Y. Influenza A virus NS1 protein activates the phosphatidylinositol 3-kinase (PI3K)/Akt pathway by direct interaction with the p85 subunit of PI3K. J Gen Virol 2007;88:13–8.
[80] Silve S, Dupuy PH, Ferrara P, Loison G. Human lamin B receptor exhibits sterol C14-reductase activity in Saccharomyces cerevisiae. Biochim Biophys Acta 1998;1392: 233–44.
[81] Simon PF, Mccorrister S, Hu PZ, Chong P, Silaghi A, Westmacott G, et al. Highly pathogenic H5N1 and novel H7N9 influenza A viruses induce more profound proteomic host responses than seasonal and pandemic H1N1 strains. J Proteome Res 2015;14: 4511–23.
[82] Simos G, Georgatos D. The inner nuclear-membrane protein P58 associates invivo with a P58 kinase and the nuclear lamins. EMBO J 1992;11:4027–36.
[83] Spicer V, Yamchuk A, Cortens J, Sousa S, Ens W, Standing KG, et al. Sequence-specific retention calculator. A family of peptide retention time prediction algorithms in reversed-phase HPLC: applicability to various chromatographic conditions and columns. Anal Chem 2007;79:8762–8.
[84] Stephens L, Anderson K, StokoeOKOE D, Erdjument-Bromage H, Painter GF, Holmes AB, et al. Protein kinase B kinases that mediate phosphatidylinositol 3,4,5-trisphosphate-dependent activation of protein kinase B. Science 1998;279:710–4.
[85] Su WC, Chao TC, Huang YL, Weng SC, Jeng KS, Lai MMC. Rab5 and class III phosphoinositide 3-kinase Vps34 are involved in hepatitis C virus NS4B-induced autophagy. J Virol 2011;85:10561–71.
[86] Taubenberger JK, Hultin JV, Morens DM. Discovery and characterization of the 1918 pandemic influenza virus in historical context. Antivir Ther 2007;12:581–91.
[87] Teijaro JR. The role of cytokine responses during influenza virus pathogenesis and potential therapeutic options. Curr Top Microbiol Immunol 2015;386:3–22.
[88] Tian Q, Stepaniants SB, Mao M, Weng L, Feetham MC, Doyle MJ, et al. Integrated genomic and proteomic analyses of gene expression in mammalian cells. *Mol Cell* Proteomics 2004;3:960–9.
[89] Tong SX, Li Y, Rivailler P, Conrardy C, Castillo DAA, Chen LM, et al. A distinct lineage of influenza A virus from bats. Proc Natl Acad Sci U S A 2012;109:4269–74.
[90] Voukkalis N, Koutroumani M, Zarkadas C, Nikolakaki E, Vlassi M, Giannakouros T. SRPK1 and Akt protein kinases phosphorylate the RS domain of lamin B receptor with distinct specificity: acombined biochemical and in silico approach. Plos One 2016:11.
[91] Walsh KB, Teijaro JR, Rosen H, Oldstone MBA. Quelling the storm: utilization of sphingosine-1-phosphate receptor signaling to ameliorate influenza virus-induced cytokine storm. Immunol Res 2011;51:15–25.
[92] Watanabe T, Watanabe S, Kawaoka Y. Cellular networks involved in the influenza virus life cycle. Cell Host Microbe 2010;7:427–39.

[93] Xi QR, Cuesta R, Schneider RJ. Tethering of eIF4G to adenoviral mRNAs by viral 100 k protein drives ribosome shunting. Genes Dev 2004;18:1997–2009.
[94] Ye Q, Worman HJ. Interaction between an integral protein of the nuclear envelope inner membrane and human chromodomain proteins homologous to *Drosophila* HP1. J Biol Chem 1996;271:14653–6.
[95] Ye QA, Callebaut I, Pezhman A, Courvalin JC, Worman HJ. Domain-specific interactions of human HP1-type chromodomain proteins and inner nuclear membrane protein LBR. J Biol Chem 1997;272:14983–9.
[96] Yeganeh B, Ghavami S, Rahim MN, Klonisch T, Halayko AJ, Coombs KM. Autophagy activation is required for influenza A virus-induced apoptosis and replication. Biochim Biophys Acta 2018 Feb;1865(2):364–78 (29108912).
[97] Zeigerer A, Gilleron J, Bogorad RL, Marsico G, Nonaka H, Seifert S, et al. Rab5 is necessary for the biogenesis of the endolysosomal system in vivo. Nature 2012;485:465–70.